Physics and applications of low energy muons

Elvezio Morenzoni

Paul Scherrer Institut, Switzerland

1 Introduction

Among the various nuclear solid state techniques, muon spin research (μSR) is a relatively young technique. However, as with all fields of science, also in applied muon science novel methods and techniques have to be developed and the capabilities of the existing ones continuously extended in order to face the challenge offered by new objects of investigations. These developments in methodology are often driven by the needs of research communities. Conversely, the availability of new scientific instruments and methodologies leads to progress in scientific knowledge. An example is the discovery of the surface muon production mechanism (Pifer *et al.* 1976). Surface muons, which originate from pions decaying at rest at the surface of a pion production target, offered decisive advantages with respect to the previously used muons obtained from the decay in flight of pions such as high degree of polarization, high stopping rate, and limited penetration depth (a fraction of a millimetre to 1mm) in relatively small specimens and gave a large impetus to μSR.

In the last decade, thin films, nanomaterials, multilayered compounds, and generally objects of restricted dimensionality have emerged as critical elements in science and technology. Different methods and particle probes such as polarized electrons, neutrons, photons, and positrons, traditionally used in condensed matter studies, have been applied to the study of these objects. The muon (μ^+) as a microscopic magnetic probe and muonium (Mu) as a light hydrogen probe are predestined to be used in these new fields. However up to now, μSR, due to the energy range of available polarized muons limited to kinetic energies of a few MeV and above, has been restricted to the study of bulk matter properties.

To be useful in thin-film and surface investigations muon beams with energies in the range of eV to several keV are needed. At these energies, implantation depths into materials range from the subnanometer to the hundred nm region. We call these beams generically low energy (LE) muon beams. There is quite a bit of confusing terminology used up to now in the context of the various LE beam developments. To clarify terms frequently used in this work and as a guide for a new reader, I think it is convenient to

bring some order in the variety of adjectives attributed to the muons offered by these new types of beams. I will loosely define the corresponding energy ranges as follows. Fast muons are the normally available muons, used for instance in conventional mSR studies, *i.e.* , muons with some MeV kinetic energies. Slow muons apply to muons with energies of several keV. Very slow will be used as synonymous of epithermal and corresponds to energies lower than about 50 eV such as the muons generated by the moderation technique in condensed van der Waals gases. Ultraslow muons are subelectronvolt muons produced for instance by laser ionisation of hot muonium. I think we should reserve the terms cold and ultracold, frequently (mis)used in the context of low energy muons, to particles with energies of the order of 200 K and much lower than this value, respectively.

Various methods to extend the range of applicability of the μSRmethod have been proposed during the last decade particularly for condensed matter investigations. These investigations require large flexibility in the choice of the experimental parameters. These conditions can be obtained only with spatial separation between muon source and sample. For other experiments, such as for instance investigations of exotic atoms formed by the capture of negative muons into an atomic orbit, the slowing down section can be integrated in the experiment. In this case different methods to slow down the muons and hence increase the stopping density and formation probability have been developed (see Simons *et al.* 1992 for an overview). In this paper I will concentrate on the characteristics and applications of LE muons obtained by the moderation of a surface muon beam. At least at the moment, moderation is the method of choice to produce polarized very slow μ^+. It is a reliable technique, simple both from the technological and operational point of view, and requires only reasonable investments.

2 Methods to produce low energetic muons

Compared to the case of other less exotic particles, for the production of low energetic μ^+, one is faced with more arduous initial conditions, which are inherent in the physics of the muon generation. The muon originates by pion decay as an energetic particle and therefore one of the first unavoidable steps toward a low energy beam is the slowing down of MeV muons. Compared to electron, proton, or ion beams, the phase space properties (beam size, divergency, density) of a typical μ^+ beam are quite poor with beam spots of several cm^2 and divergencies of the order of 100mrad. This is a consequence of the source of muons not being spatially concentrated and of the limited lifetime. The intensities of beams (for surface muons typically between 10^5 and 10^8 μ^+/s) are many orders of magnitude lower than those of stable particles, a reality reflected by the fact that one expresses beam intensities in particles per second instead of the usual units of current.

2.1 Use of degraders

In principle, a straightforward way to obtain low energy positive muons is to tune a conventional surface muon beam line to momenta much lower about 29MeV/c. In this case those muons are collected and transmitted that originate from pions stopped at some depth from the surface of the carbon production target. By traversing this amount of material, the muon loses energy because of inelastic and elastic collisions with the

constituents of the target. Besides energy degradation, absorption also takes place. The muon intensity $N(p)$ at the end of a typical surface muon beam line has the following momentum dependence

$$N(p) \cong \frac{N_s p^{3.5} \exp\left[-m_\mu l/p\tau_\mu\right]}{29^{3.5}}, \qquad 5 \leq p \leq 29\text{MeV/c} \tag{1}$$

where p is the momentum in MeV/c, l the length of beam line, t_μ the muon lifetime, m_μ the μ^+ mass, and N_s the intensity at 29MeV/c. This method provides reasonable beam intensities and manageable background rates only down to a few hundred keV of kinetic energy (Badertscher *et al.* 1985). Below this energy, the decrease in intensity is more pronounced than the one predicted by Equation 1. Multiple scattering and energy straggling in the degrader strongly reduce the phase space density of the emerging particles. Transport, energy selection, and focusing of these particles to an experiment or to a sample are very inefficient so that no practical flux intensity is obtained. The background level from positron contamination, roughly independent of the particle momentum (see Figure 1), is also a disturbing factor.

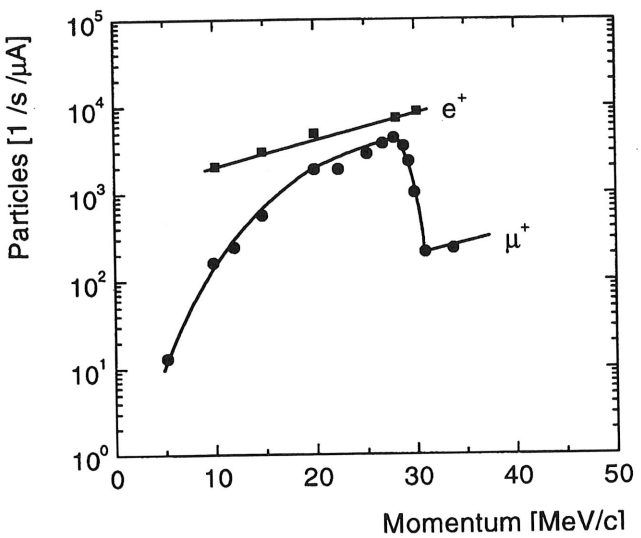

Figure 1. *Typical momentum dependence of the intensity of a positive muon beam. Three components can be recognized: the surface muons (edge at 29.8MeV/c), the subsurface muons (below the edge momentum), and the rest, given by muons from pions decaying in flight and acquiring energies lower or greater than the muon decay energy.*

Degrading a surface muon beam in a low Z metallic material near the experiment could circumvent part of the transport and lifetime losses. This scheme corresponds to moving the outer part of the production target close to the experiment. However, this method also does not produce encouraging results. Figure 2 shows for instance the energy distribution after a degrader whose thickness was optimized for maximum slow muon intensity. As a consequence of the statistical nature of the slowing down process, a broad energy distribution of the exiting particles is found. Energy selection of such a

beam by electrostatic or magnetic analyzers would lead to unacceptable intensity losses. Below 30keV the yield of μ^+ exiting the degrader is very low since, at this energy, muons exiting the degrader preferably capture an electron and form Mu. The probability of Mu formation increases with decreasing energy reaching almost 100% at a few keV (Prokscha *et al.* 1998). Moreover, because of the electronic interactions of very slow μ^+ in a metal, such a scheme is not able to create a flux of particles with a few eV energy (see Section 4).

Figure 2. *Energy dependence of surface muons emerging from an Al degrader. The thickness of the degrader has been chosen to optimize the intensity of muons with energy lower than 30keV. The full circles indicate the muonium component.*

2.2 Phase space compression

Phase space compression by stochastic or electron cooling has been successfully applied to stored beams of protons and heavy ions to improve the beam quality and is routinely used at various accelerators. In stochastic cooling, appropriate pick up elements determine beam parameters (such as for instance lateral dispersion) from a sample of particles. In a successive step, according to the measured values, a correction is applied to reduce the spread. One can show that, by repeating this process several times, the beam as a whole is cooled and a phase space compression is obtained (van der Meer 1985). Stochastic and electron cooling, where the cooling is obtained by reducing the beam temperature through the interaction with an electron beam at lower temperature, although effective, are too slow for unstable particles like the muons, where a rapid action is required within the lifetime. To circumvent this limitation, a method was proposed where each particle is treated separately (Taqqu 1986). This can be considered as the limit case of the stochastic cooling method and defined as single particle cooling.

The basic idea is to measure the position of each particle in the 6-dimensional phase

space and to move the coordinates to a desired position in the phase space with pulsed electromagnetic deflection and steering systems. This way, a beam with low energy and good phase space properties can be envisaged. The cycle, measurement-steering-measurement, has to be repeated many times and the process has to be divided into various consecutive stages, each one responsible for a phase space compression, deceleration, or for the optimal preparation of the particle for the next stage. The development of such a machine represents a formidable technological challenge and requires substantial investments. The results of experiments performed at the Paul Scherrer Institute (PSI) (Fuchs 1992, Simons *et al.* 1992) have indicated that the required accuracy and high repetition rates of phase space measurements and correction cannot be achieved at the present state of technology and that the method cannot be used to decelerate effectively existing beams of muons with kinetic energies in the MeV region. The method was not successful in producing a low energy beam. Nevertheless, the results obtained in the study indicate that specific elements of such a technique implemented in a beam line of muons that have previously been slowed down to energies in the region of a few tens of keV could provide a sizable improvement of the beam quality.

2.3 Ionisation of thermal muonium

In selected materials, such as hot noble metals (W, Pt, Ir or Re) or low density silica powder (SiO_2), a fraction of implanted surface muons (0.01–0.05 in metals and up to 0.10 in SiO_2), after reaching thermal energies, diffuses to the surface and is reemitted as thermal muonium (Mills *et al.* 1986a, Beer *et al.* 1986, Matsushita and Nagamine 1996). The exiting atoms can be ionized by multiple photon excitation produced by appropriate lasers (Chu *et al.* 1988) thus resulting in thermal μ^+ , which can be used as a source of a low energy beam. This scheme, proposed in 1987 (Nagamine 1987), is being developed at the Meson Science Laboratory of the High Energy Accelerator Research Organization (KEK, Japan). The method is only applicable at a pulsed beam line where the laser can be efficiently synchronized with the accelerator delivering bunches of muons. The ionisation is obtained by exciting the 1s electron into a 2p state and from here to the continuum. To maximize the intensity of low energy muons, the primary production material (BN), where the pions are created and decay, and the thermalising foil (hot W), where the muons are stopped and emitted as thermal Mu, are accommodated in a single layered target directly inserted in a pulsed proton beam line (Silica powders have proven to be the most efficient $\mu^+ \rightarrow$ Mu converter, but the impinging proton beam provides a too adverse environment for this type of target). This technique produces a source of ultraslow μ^+ with an energy of 0.2 eV, which are then extracted and accelerated toward the sample region (Figure 3). Recently, the first successful production and collection of μ^+ by this method (at a rate of $0.2\mu^+/s$) was demonstrated (Nagamine *et al.* 1995) (Figure 4).

2.4 Moderation

A moderator is to some extent a very specialized degrader. Differently from a degrader, a moderator is able to deliver a source of thermal or epithermal particles by efficiently converting high energetic particles into thermal particles or into very slow ones with energies of a few eV. It relies on specific properties of the interaction and of the transport

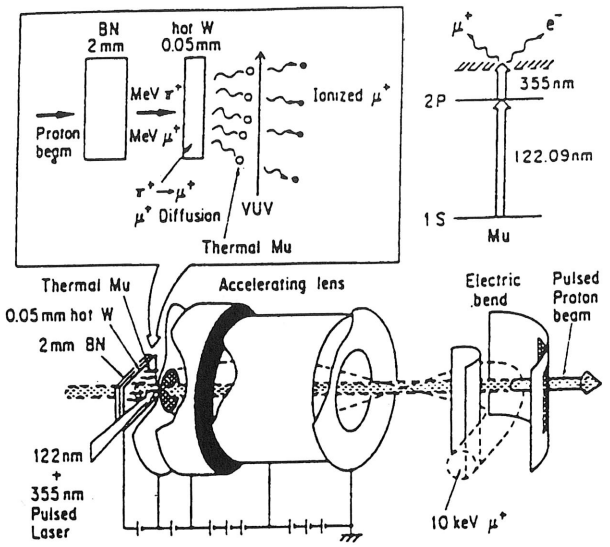

Figure 3. *Schematic view of the experimental arrangement for ultraslow muon production at KEK. Thermal muonium, produced from a hot W foil using pulsed 500 MeV protons, is ionized by a laser. The insets show a schematic view of the mechanism for the ultraslow muon production and the muonium energy levels and laser lines involved in the resonant ionisation.*

of thermal or epithermal particles in appropriate solids, which lead to an unusual large emission probability of particles slowed down in these materials.

Moderation is routinely used in the production of eV or sub-eV positrons and in the corresponding low energetic beams. In analogy to the case of muons, the particles to start with are of energetic nature. Positrons are obtained from β^+ radioactive sources or from pair production in accelerators and have energies comparable to mc^2=511keV. An energetic positron entering a metal moderator is rapidly slowed down in a time of the order of picoseconds until it reaches thermal equilibrium with the surrounding crystal. Moderation is caused well above thermal energy by collisions with free or bound electrons and, near thermal energies, by positron-phonon interactions. Some of the thermalized e^+ may diffuse to the metal-vacuum interface within their lifetime and be reemitted. The reemission is due to a negative work function Φ_+ in the corresponding materials and ejected e^+ have a kinetic energy of $-\Phi_+$, blurred by the thermal motion. Metals where positrons have a negative work function form the key component of low energetic positron beams in many laboratories throughout the world. A very efficient and practical moderator has proven to be hot single-crystal tungsten of high purity, where the e^+ are not trapped in defects and the diffusion length is high. The efficiency of these processes is defined as $\epsilon = N_{\mathrm{eV}}^{\mathrm{out}}/N_{\mathrm{Mev}}^{\mathrm{in}}$. Depending on the set-up, efficiencies of up to a few parts per thousand can be achieved but more typical efficiencies are of the order of 10^-4 (Schultz and Lynn 1988).

This is not the only mechanism for positron emission. Moderators not relying on a

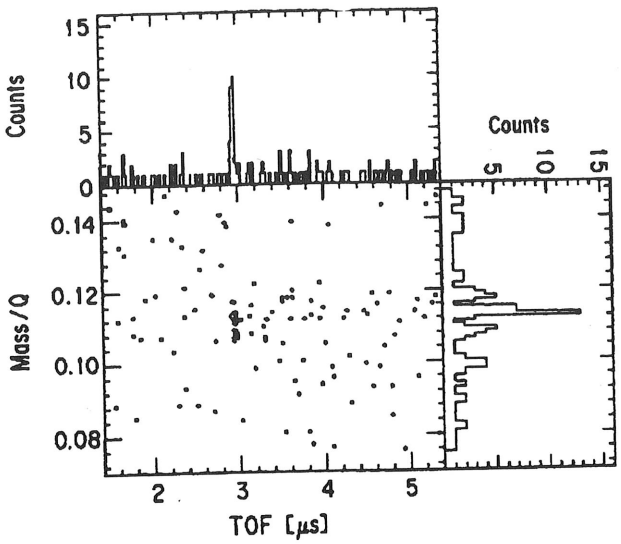

Figure 4. *Two-dimensional mass-time-of-flight spectrum showing the generation of ultraslow μ^+ by laser resonant ionisation of muonium. The peak corresponds to ultraslow μ^+ produced near the W foil, accelerated, and transported to a microchannel plate detector at the end of the low energy μ^+ beam line (Nagamine et al. 1995).*

negative work function also exist. For instance, e^+ injected into ionic crystals have been found to be reemitted with kinetic energies peaked at some eV (Mills and Crane 1984). Rare gas solids (RGS), also exhibiting positive work function, have high, but widely varying moderation efficiency with typical values around 10^{-3} and reported values up to the order of a percent (Jääskeläinen *et al.* 1997). For these wide-band-gap insulators, the general picture of the dynamics is described in terms of emission as a result of inefficient cooling below the Ps formation threshold. However, various questions remain and not all the factors governing this behavior have been identified.

The large amount of empirical data about e^+ moderators that has been collected over the years can be used as guidance to predict expected properties of muon moderators. However, the different mass of the two particles leads to important differences in their physical properties (energy spectra, size, and binding energy of neutral fraction, etc.) and their dynamical behavior in condensed matter. Even at thermal energies the muons behave mostly as well-localized classical particles (de Broglie wave length at room temperature $\lambda_{dB} \approx 0.4$nm), whereas for positrons the wave character is dominant already at eV energies ($\lambda_{dB}(1\text{eV}) = 1.2$nm). Being more delocalized, we expect the positron to be more affected by interactions with moderator defects or voids than the muon, where it may become trapped or localized and annihilate with electrons. The interaction with phonons is much more important and positron diffusion rates are much larger than those of muons.

The problem of positron moderation has a long tradition and was first investigated as long ago as 1958 (Cherry 1958). The fact that positrons are easily obtained from radioactive sources has facilitated the development of low energy beams throughout the world.

Nowadays, moderation is the method of choice to build a source of very slow positrons and practically all low energy beams realized up to now are based on moderators (very often the practical tungsten) or contain at least a moderation section. Particularly in the last decades, the physics of positron thermalisation and emission, the related developments, and their use have received considerable attention. By contrast, studies of muon moderation are very scarce. Moderation of surface muons to epithermal energies was first shown at the TRIUMF meson factory (Canada) (Harshman *et al.* 1986 and 1987). The second important step was the demonstration that the moderation process fully conserves the initial polarization of a surface beam (Morenzoni *et al.* 1994). This opened the way to the development of beams of polarized low energy muons, the first of which has been realized at a continuous surface muon beam at the Paul Scherrer Institute (Switzerland) (Morenzoni *et al.* 1997a). Very recently, the development of a similar beam based on the pulsed ISIS source at the Rutherford Laboratory (UK) has also been initiated.

3 Characteristics of moderated muons

3.1 Experimental details

The principle of the moderation method is shown in Figure 5. Surface muons from a secondary beam (originating from the proton beam striking the production target) impinge on a moderator from the back side. The low energy beam is formed by collecting at the downstream side very slow muons that escape from the moderator and represent the source of a tertiary beam. Figure 6 shows the layout of the LE muon beam realized at PSI. We give here only some experimental details for better understanding of this section and refer to Morenzoni *et al.* (1997b) and Section 5 for more details. The main components are recognizable: the moderator, the electrostatic acceleration and transport section, the retractable detector for LE-μSR experiments (trigger detector), and the sample region with magnet and μSR spectrometer. The moderator section can be cooled by a He flow cryostat down to approximately 7K. This allows the deposition on a thin substrate of a few 100nm thick layer of a van der Waals bound solid, which has proven up to now to be the most efficient μ^+ moderator. The total thickness of the material traversed by the surface μ^+ and the exact incident beam momentum are chosen so that the stopping density distribution of the μ^+ is centered at the downstream surface of the target, *i.e.* , in the condensed gas layer. This optimizes the very slow muon yield and means that in the moderator (essentially in the substrate) about 50% of the beam is stopped. To avoid surface contamination of the moderator, ultrahigh vacuum (UHV) technology with bakable stainless-steel chambers sealed with copper gaskets is used for the whole apparatus (typical pressure 10^{-10}mbar). The substrate with the moderator is electrically insulated and can be raised to voltages as high as 20 kV. This allows the acceleration and extraction of the very slow μ^+ from the production region and is one possible method to select the energy of the tertiary beam (see also Section 5). The acceleration takes place in a two-stage system formed by the substrate and two wire planes. The slow muons are deflected by 90 degrees with respect to the incoming fast μ^+ by means of an electrostatic mirror and are focused by electrostatic "einzel lenses" onto the sample position.

To study the characteristics of the muons exiting the moderator, the trigger detector is retracted and a position sensitive microchannel plate (MCP2 in Figure 6) is mounted

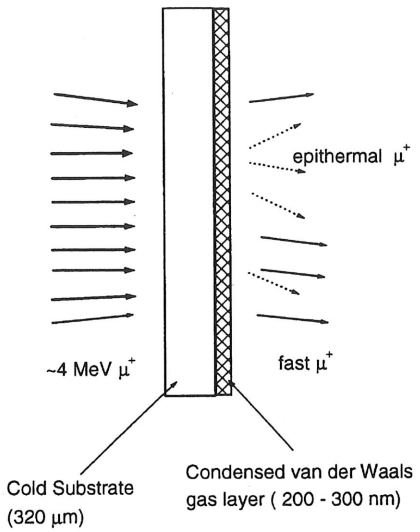

Figure 5. *Principle of the moderation technique for the production of very slow polarized μ^+. The total thickness of the moderator is chosen to maximize the yield of epithermal muons.*

instead of the sample. The muons can be unambiguously identified using the signal of this detector in coincidence with the delayed signal from one of the four pairs of scintillators. These are shaped as cylindrical sectors and detect the positron originating from the μ^+ decay at the MCP2 (or sample) position.

The epithermal muons appear as a pronounced peak in the time-of-flight (TOF) spectrum started by the fast muons traversing the entrance scintillator and stopped by the slow μ^+ deflected and focused onto MCP2. A sizable very low energy component appears only if a condensed layer of a van der Waals gas is deposited on the substrate. This is clearly demonstrated in Figure 7. The dark histogram shows a TOF spectrum obtained by moderating the μ^+ in a bare metal substrate. A broad continuum is observed corresponding to degraded muons with energies ranging up to the maximum energy that can be deflected by the electrostatic mirror. The other histogram shows the TOF spectrum measured with a thin Ar layer deposited on the substrate, normalized to the same number of incident muons. In addition to the broad continuum, the Ar spectrum has a much narrower and stronger component corresponding to very slow μ^+ emitted from the Ar layer. The difference between the two distributions is impressive and directly points out the special role played by the thin condensed layer. A similar TOF spectrum obtained with a pulsed surface muon beam at ISIS is shown in Figure 8 (K. Träger *et al.* 1998).

3.2 Energy distribution

The basic quantity to describe the emission phenomena is the number of muons with energy E emitted per second and cm^2 from the moderator surface in the direction $\mathbf{\Omega}$. This quantity, normalized to unit current of the fast muons impinging on the moderator, is an energy and angle dependent current density $j(E, \mathbf{\Omega})$.

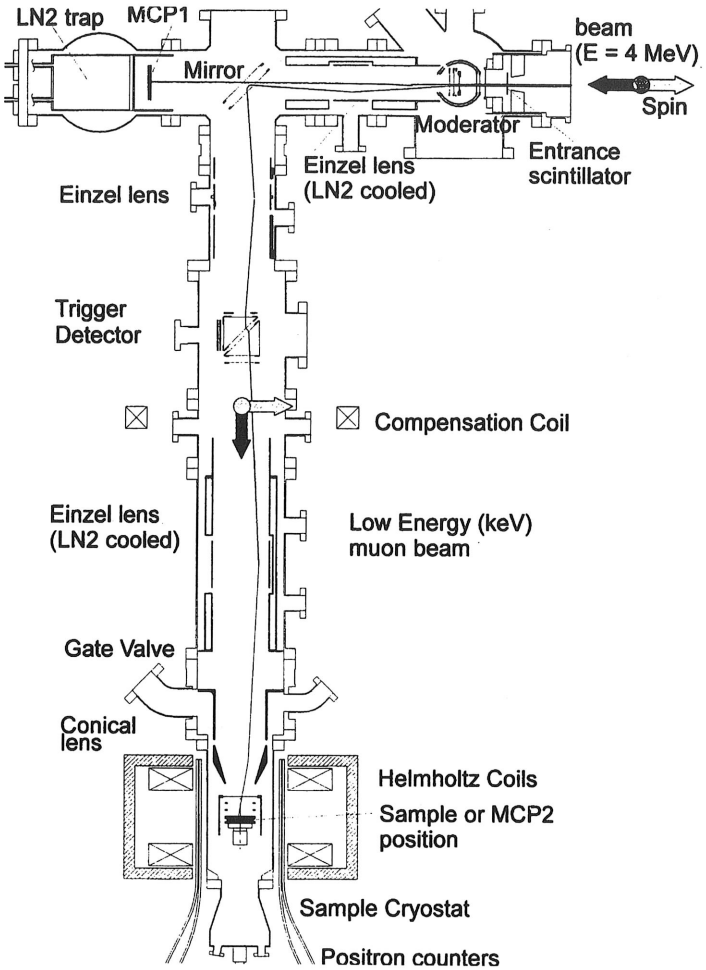

Figure 6. *Layout of the low energy polarized muon beam at PSI used for LE– μSR and other applications.*

In principle, the maximum information about the moderation process could be obtained by measuring directly this double differential quantity, but this task is not manageable in the case of muon emission. The actual experimentally accessible quantities are integral quantities such as the energy distribution

$$j(E) = \int j(E, \mathbf{\Omega}) d\Omega, \tag{2}$$

the angular distribution

$$j(\mathbf{\Omega}) = \int j(E, \mathbf{\Omega}) dE, \tag{3}$$

and the moderation efficiency

$$\epsilon = \int j(E, \mathbf{\Omega}) dE \, d\mathbf{\Omega}, \tag{4}$$

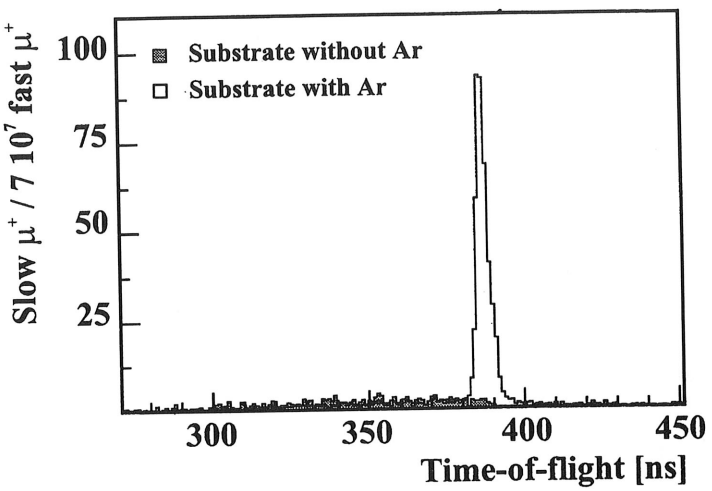

Figure 7. *Time-of-flight spectrum between start scintillator and MCP2 showing slow and very slow μ^+. Dark area: bare substrate as moderator. White area: thin layer of solid Ar evaporated on the substrate. Both curves are normalized to the same number of incoming surface muons. The peak clearly shows the emission of very low energy μ^+ from the solid Ar surface.*

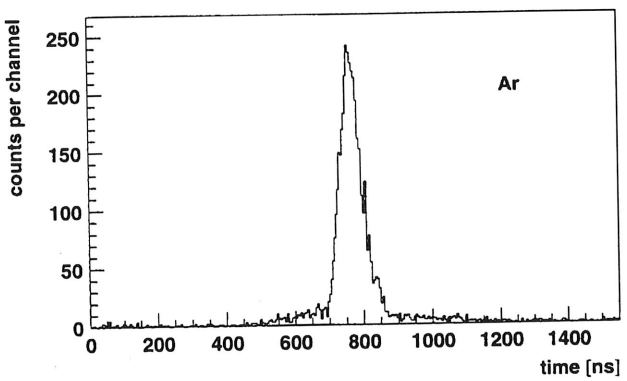

Figure 8. *Time-of-flight spectrum of muons emitted from solid Ar after moderation of the pulsed surface muon beam at ISIS. The muons have been accelerated to 8keV.*

To characterize ϵ the momentum p and momentum width Δp of the incident μ^+ must be specified, as well as the geometry of the moderator and in principle the angle of impact of the energetic particles with respect to the surface of the moderator. In this work we deal only with normal incidence.

The procedure for the determination of the energy distribution consists of several iterative steps, which also involve the determination of the angular distribution (Hofer 1998). Essentially, it is based on simultaneous fits of measured TOF spectra between

moderator surface and MCP2 detector with corresponding distributions generated by Monte Carlo simulations. Measurements at constant moderator bias are performed as a function of the potential between the moderator surface and the first grid of the extraction system. At very low extraction fields the muons exiting the moderator are first very smoothly accelerated thus greatly enhancing the sensitivity of the time-of-flight on the distribution of initial energies. An example of the TOF distributions is shown in Figure 9 in the case of a solid Ar (s-Ar) moderator. Decreasing the extraction voltage shifts the distribution to longer times and makes it wider, indicating that the spectrum contains a sizable low energy component. Superimposed to the measured TOF spectra are the results from the fit procedure. The corresponding energy spectrum up to 3 keV is shown in Figure 10.

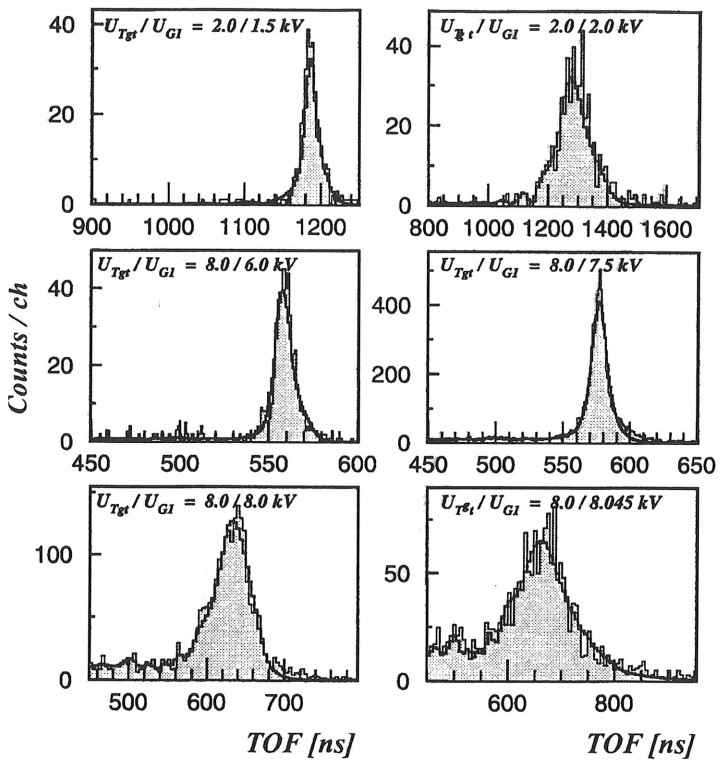

Figure 9. *Time-of-flight distribution of very slow muons emitted from the moderator at various extraction voltages (U_{mod}/U_{grid}). The thick line gives the result from the Monte Carlo simulation and the fit procedure used to determine the energy distribution.*

Figure 11 shows the normalized distributions from zero to 100eV from different moderators. The distribution is dominated by a broad peak centered at 15eV, extending from 0 to about 30eV (FWHM 20 eV) and a flat tail to higher energies. The energy of the muons contained in the peak is well above the thermal energy and classifies them as epithermal. Within the rare gas solids, the integral number of counts in the peak increases with decreasing atomic number, reflecting the corresponding variation of the moderation

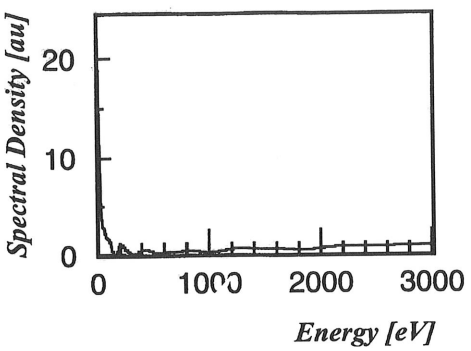

Figure 10. *Energy spectrum of slow muons emitted from solid Ar between 0 and 3000eV.*

efficiency. Since the energy resolution of the method is limited to a few eV, it is not possible to resolve features that may correlate with specific electronic excitation channels of the target atoms or different threshold mechanisms. Within the experimental error, muons exit different van der Waals bound solids with similar energy distribution but different emission probability. The Al and SiO_2 spectra are representative of other metals and solid insulators, respectively. A comparison of the energy distributions of muons emitted from van der Waals cryosolids with those of muons emitted from metallic or solid insulators evidences a completely different behavior. In contrast to van der Waals bound solids, these materials do not show a sizable epithermal component. Only the structureless energy distribution of the accompanying high energy tail is observed and very few muons with energies lower than 30eV are emitted from these materials. These distributions as well as the yield measurements presented in Section 3.6 clearly indicate that the emission of very slow muons is a mechanism peculiar to van der Waals condensed gases and that only these materials seem to possess true moderating properties for muons.

3.3 Angular distribution

A comparative study of very slow muon yields from moderators grown under identical conditions, but with different geometry can be used to determine the angular distribution of epithermal muons. Particularly instructive is the comparison of the efficiency of a flat substrate configuration with that of a structured substrate configuration. An example of the latter is shown in Figure 12 obtained by etching a Si wafer along the [111]-plane. This substrate possesses the same projected surface F than the flat one, but an increased active area A

$$A_{\text{struct}} = \frac{F}{\sin\alpha} = 1.73 A_{\text{flat}} \tag{5}$$

where α is the angle defined by the etching direction with respect to the surface normal. As expected from simple geometrical considerations, depending on the angular distribution of the muons, the increase of the active area may lead to an increase of the normalized yields of slow muons. It is easy to recognize that, in the case of extreme forward emission, only the projected area is determinant and no difference is expected between structured

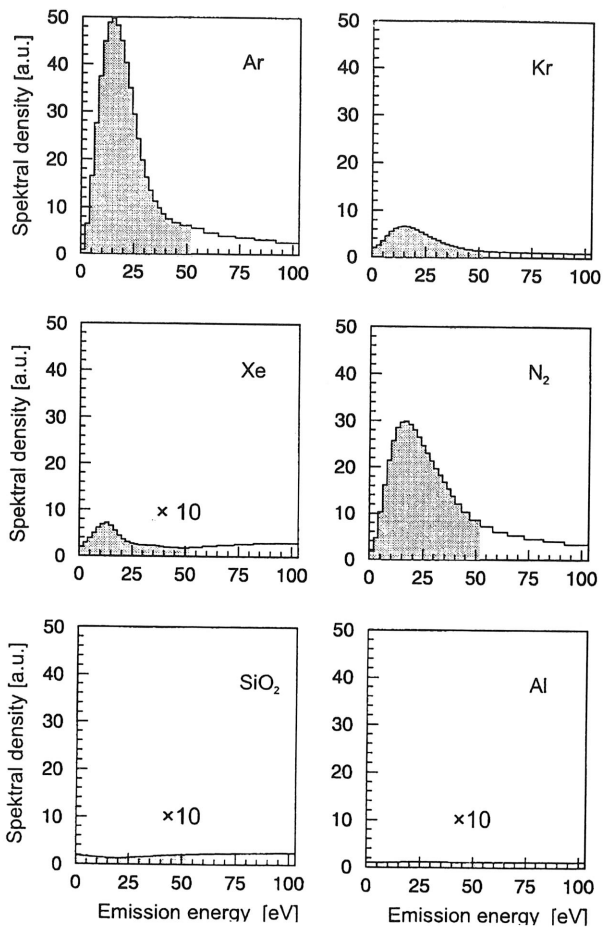

Figure 11. *Energy distribution of very slow muons from various moderators. The zero on the energy scale corresponds to the energy outside the moderator. The spectra are normalized to the same number of incoming fast muons.*

and flat substrates. The opposite case of internal isotropic distribution (*i.e.* external cosine distribution) gives rise to a yield enhancement equal to the active area ratio. Experimentally we find for a s-Ar moderator an enhancement factor of 1.7±0.1, in good agreement with the prediction of a cosine angular distribution of emission. Solid N_2 gives similar results.

Additional evidence for a cosine distribution comes from the transport properties of the epithermal muons. The transport efficiency from moderator to sample position depends on the initial divergency and hence on the angular distribution. A detailed comparison of measured transport efficiency as a function of the transport settings with simulated efficiencies assuming different angular distributions shows that the experimental data are well reproduced by a $\cos\theta$ distribution. (We have examined the sensitivity of the energy distribution on the angular distribution and vice versa. A comparison with the experimen-

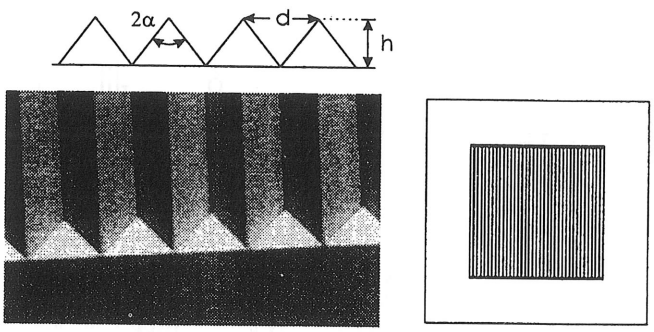

Figure 12. *Electron microscope image of a structured silicon substrate used to increase the active moderator area. Ridge pitch is about 30mm and ridge height 20mm.*

tal data shows that the given distributions represent the best choice. Significantly poorer agreement is obtained with other combinations of distributions—Hofer 1998). The externally measured flux of emitted muons obeying a cosine distribution reflects an isotropic internal distribution of velocities irrespective of the presence of a possible energy barrier at the surface. The mechanisms leading to the diffusion-like behavior of the epithermal muons inside wide-band-gap cryosolids are discussed in Section 4.

3.4 Polarization

One of the most important properties of the epithermal muons is their polarization. In principle information on magnetic moments of the surface can also be obtained with unpolarized particles (for instance by scattering slow muons at grazing incidence and measuring the Mu formation probability in the triplet and singlet state). However, it is evident that, for an unrestricted use of moderated muons as magnetic microprobes, they should be polarized, since the quality factor of a μSR signal is proportional to the square of the polarization. This important parameter has been measured in various transverse field LE–μSR experiments, by stopping the moderated μ^+ in targets where the behavior of the thermalising muons is known. In the first experiment we used a MCP as an active target to start the time differential μSR experiment (Morenzoni *et al.* 1994). Later, we remeasured the polarization by using the LE–μSR set-up described in Section 5 and implanting the μ^+ in very pure Ag, or Cu samples. Figure 13 shows for example an asymmetry spectra of μ^+ in Ag.

The results from the different experiments show that moderation of surface muons and emission of epithermal muons from van der Waals bound solids (Ar, N_2, and Kr) conserve, within the experimental error of 5–10%, the nearly full initial polarization. The result has important physical implications and narrows spectrum and time scale of the processes playing a role in the generation and emission of very slow particles. The measurement of the energy distribution classified them as epithermal, but did not permit to discriminate uniquely between possible different production mechanisms. The experimental time resolution of the TOF measurements sets an upper limit of 10^{-9}s between implantation of the fast muons in the moderator and reemission of the very slow

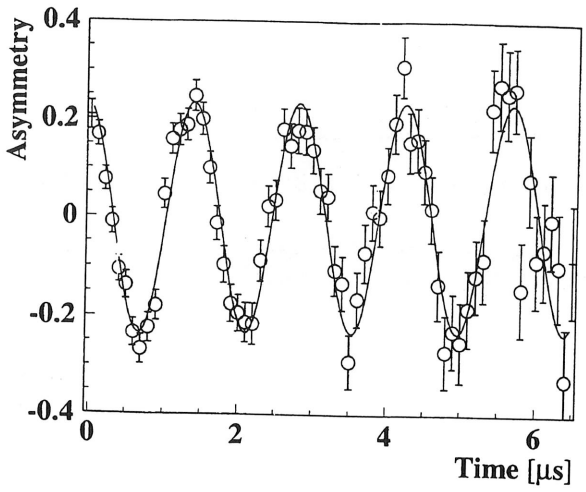

Figure 13. *Asymmetry signal from the decay of 16keV muons stopped in an Ag foil and precessing in a 5mT transverse magnetic field. The asymmetry plot has been obtained from the Left-Right decay spectra (corrected for random background and solid angle effects) by forming the ratio* $A_{LR} = (L - R)/(L + R)$. *This removes the muon lifetime and allows to view directly the time dependence of the polarization of the muon ensemble.*

muons. However, this limit per se does not exclude diffusion controlled emission of μ^+, which was originally proposed on the base of an analogy with e^+ emission from solid moderators (Harshman *et al.* 1986, Mills *et al.* 1984). According to this recombination-assisted diffusion mechanism, the very slow μ^+ are produced from the break-up near the moderator surface of muonium that is formed inside the solid. Muonium can acquire energy by catalyzing a first electron-hole recombination. A second recombination between the bound Mu electron and another hole near the surface causes the muonium to break up and a μ^+ with several eV of kinetic energy to be reemitted. However, this interpretation is questionable since it necessitates the assumption of a high density of states at surfaces and needs an unlikely transfer of energy from a third body to explain the large hyperthermal energy.

The observation that the very slow μ^+ practically retain the full initial polarization gives direct evidence against these mechanisms since it implies an upper limit to the time scale of the processes responsible for the moderation. In solid Ar , Kr, and Xe thermalisation leads to practically 100% muonium formation. In solid N_2, too, more than 80% of the muons thermalise as muonium. Since the polarized muon captures unpolarized electrons from the moderator, muonium can be produced with equal probabilities in two different spin states: ortho-muonium in which the muon and electron spins are parallel at the time of the bound state formation and para-muonium in which the spins are antiparallel. The muon spin polarization is not affected by the ortho-muonium formation, because the ortho-muonium is an eigenstate of the muonium hyperfine Hamiltonian in zero magnetic field. However, para-muonium is not an eigenstate and oscillates between a triplet (F=1, M=0) and the singlet (F=0, M=0) eigenstates with the muonium hyperfine frequency $\nu_{\rm hf}$ of 4463MHz (F is the total muonium spin and M is the projection on the

quantization axis). The evolution of the muon polarization with time Δt after muonium formation is expressed by:

$$P(t + \Delta t) = \frac{1}{2} P(t)(1 + \cos \omega_{\mathrm{hf}} \Delta t). \tag{6}$$

Every time muonium is formed in the antiparallel spin state, the muon spin rotates by a factor $\cos(\omega_{\mathrm{hf}} \Delta t)$. The existence of para-muonium during moderation for times comparable or larger than the hyperfine period ($T = 2\pi/\omega = 224$ps) would depolarise the muon spin. Therefore, delayed or slow emission processes such as those proceeding over thermalisation are at variance with the experimentally observed conservation of the polarization and can be excluded as a source of the majority of these particles.

The polarization result is consistent with epithermal μ^+ emission via hot emission processes. The observed μ^+ are particles that escape thermalisation. This conserves the initial surface μ^+ polarization since the overall time for slowing down from MeV to 10eV energies is very short (10ps) and depolarisation via muon-electron, muon-atom or muon-molecule scattering is negligible. As a result, even transient Mu formation in this regime does not give rise to noticeable depolarisation. It should be emphasized that, in contrast to the slower processes, which are observed in conventional μSR experiments, the measurement of the polarization of epithermal muons is sensitive to the presence of extremely rapid depolarisation processes. The results also show that depolarising processes in local magnetic fields or spin exchange interactions with free electrons and ions, which are produced in the wake of the slowing down $\mu+$, with magnetic moments in nuclei of isotopes, or with small quantities of paramagnetic impurities, can be excluded. No spin-lattice depolarising effects, which represent an important field of investigations of μSR experiments, are involved since they occur only after thermalisation.

Contrary to the moderation method, the generation of ultraslow muons via ionisation of thermal Mu leads to a 50% polarization loss, due to the hyperfine interaction in those muonium atoms formed with antiparallel muon and electron spin (Miyake et al 1997) (Figure 14). In this case, to recover the polarization one has to apply over the source region a longitudinal magnetic field of a few kG, enough to decouple electron and muon spin. However, the possible negative interference of such a field with the beam extraction must be taken into account.

3.5 Escape depth

An important phenomenological quantity, the escape depth of epithermal μ^+, can be obtained from the yield dependence on the thickness of the condensed gas layer. Figure 15 shows the results for Ar and Kr moderators. In both cases, the yield first linearly increases with thickness until it saturates at values of a few hundred nm, indicating that the epithermal μ^+ originate from the last 50 to 100nm of the layer. In Section 4, by describing the diffusive motion of epithermal muons in a condensed van der Waals solid, an analytical expression for the epithermal μ^+ yield $j(d)$ as a function of the condensed gas thickness d is derived (Equation 18). Using this equation to fit the data of Figure 15, an average escape depth L can be determined. We find for Ar $L = 67 \pm 5$nm and for Kr $L = 33 \pm 5$nm. Analogous measurements for N_2 give $L = 50 \pm 10$nm but for Kr unknown. The large value of the escape depths in spite of the relatively large mass of the muon is

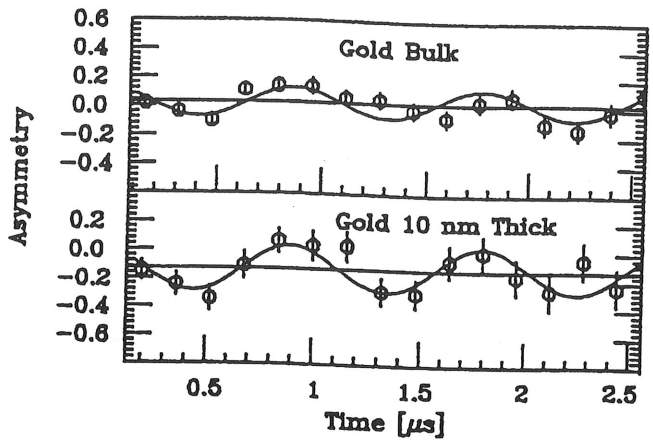

Figure 14. *Asymmetry plot of ultraslow μ^+ produced by Mu ionisation and implanted in gold (from Miyake et al. 1997).*

remarkable and is one of the elements responsible for the large moderation efficiency in these materials (see Section 4 and Equation 20). Similar or larger escape depths have been previously reported only for light particles such as hot positrons and particle or x-ray induced secondary electrons emitted from rare gas solids or ionic insulators (Gullikson and Henke 1989). However, in the case of light particles, transport and emission rest on different interaction mechanisms. For instance, excess electrons have negative electron affinity in some cryosolids (Ar, Ne and N_2) or wide band-gap insulators (MgO) and may travel in a delocalized conduction band state.

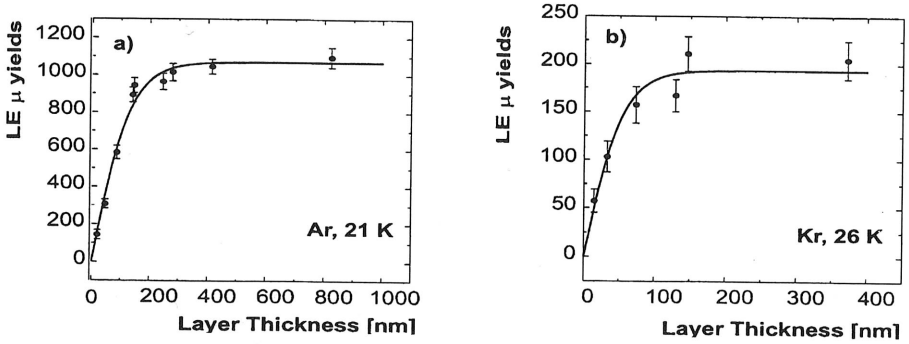

Figure 15. *Dependence of the epithermal muon yield on the thickness of the condensed gas. (a) solid Ar, (b) solid Kr. The Ar moderator was grown at 21 K at a partial pressure of 4×10^{-5}mbar and the Kr one at a temperature of 26°K and a pressure of 10^{-5}mbar. The solid line represents a fit to the data according to a diffusion model (Equation 18).*

3.6 Material dependence

In the search of the best moderator and with the purpose to understand the muon moderation dynamics, the moderation efficiency of different elements and compounds has been investigated. Table 1 summarizes the results. The materials are grouped in four classes: rare gas solids, molecular cryocrystals, solid insulators, and metals. The last column gives the energy gap of the material, which is one of the important parameters characterizing the moderating properties of a material.

Moderator	Efficiency	Energy gap [eV][a]
Ne	$1.4 \pm 0.2 \times 10^{-4}$	21.58
Ar	$8.6 \pm 1.2 \times 10^{-5}$	14,16
Kr	$1.7 \pm 0.2 \times 10^{-5}$	11.61
Xe	$5.7 \pm 1.1 \times 10^{-7}$	9.33
N_2	$6.3 \pm 1.1 \times 10^{-5}$	15.1
O^2	$1.4 \pm 0.2 \times 10^{-5}$	12.08[b]
CH4	$1.4 \pm 0.2 \times 10^{-5}$	12.51[b]
LiF[c,d]	$1.9 \pm 0.5 \times 10^{-7}$	14.1
SiO_2[e]	$3.0 \pm 1.0 \times 10^{-7}$	~9
Al	$2 \pm 0.4 \times 10^{-7}$	0
Cu[c]	$1 \pm 0.3 \times 10^{-7}$	0
St. Steel[c]	$1.4 \pm 0.3 \times 10^{-7}$	0

Table 1. *Moderation efficiency of various materials. The data are given for a beam of ~28 MeV/c momentum, momentum bite 1.5%, and a moderator with planar geometry. Notes: (a) Condensed phase values; (b) Gas phase value; (c) Values obtained from the raw spectra of Morris (1990)—they include only the epithermal component after correcting for the different beam parameters and detection efficiency; (d) Air cleaved LiF with ⟨100⟩ axis normal to the surface, moderator temperature 150° (Harshman et al. 1984); (e) SiO_2, c axis normal to the surface, T=150° , or 100nm oxide layer on Si wafer.*

Within the group of cryocrystals a strong correlation between band-gap energy and emission efficiency is observed. Elements with large band-gap energy show the highest efficiency, with solid Ne and Ar giving the highest yields. (The Ne moderator has not been as systematically optimized as Ar or N_2. Due to its very low binding energy, a thin film is stable only below ~8K. This makes Ne a relatively impractical element for large open area moderators. However, it is the moderator probably presenting the largest potential for improvement.)

This correlation is very pronounced for Ar, Kr, and Xe which display band-gap energies of 14eV or smaller. A mere reduction of 2.5eV from Ar to Kr leads to a factor of 5 reduction of the very slow muon yields. An additional decrease of 2.3eV further suppresses the efficiency by a factor of 30. As we will elucidate in Section 4, the final fate of the epithermal charge states of the muon depends primarily on the relationship between ionisation potential of the cryosolid and of muonium and on an efficient suppression of electronic excitation processes. The pronounced yield dependence reflects the special role played by epithermal electron capture leading to muonium formation inside the moderator, considerable momentum loss, and disappearance of the free epithermal μ^+ fraction .

The correlation between yield and band-gap energy is also observed in molecular cryocrystals, which exhibit slightly lower efficiencies than the corresponding atomic cryocrystals. In metals, an effective threshold for conduction electron excitation is absent. Energy can always be transferred from the μ^+ to electrons near the Fermi level exciting them to empty states in the conduction band. This causes a greater rate of μ^+ energy dissipation and consequently strongly suppresses the escape probability of very slow μ^+, which have been generated inside the metal, making these very poor moderators. An analogous behavior, though based on a different dynamics, is observed in secondary or ion induced electron emission, where the yields from insulators are much higher than from metals, which exhibit attenuation lengths for kinetic electron emission of only 1nm. Also the band-gap energy of semiconductors is too small to expect the emission of a sizable fraction of epithermal μ^+. Preliminary measurements of diamond moderation confirm this expectation. A straightforward conclusion from the results of Table 1 is that the best if not the only moderators are atomic and simple molecular cryocrystals. A wide band-gap appears to be a necessary but not sufficient condition to make an efficient muon moderator. This is clearly evidenced by the very low efficiencies observed in insulators such as LiF and SiO_2, which have efficiencies comparable to those of metals. This property points to a different dynamical behavior of epithermal muons in insulators with ionic character and will be discussed in detail in the next section.

Also the most efficient yet found e^+ moderators are solid rare gas layers, which are about an order of magnitude more efficient than annealed tungsten foils. However, the similarities with μ^+ end here. Within the rare gas solid group the elemental dependence is completely different for e^+ and μ^+ . Earlier measurements (Mills and Gullikson 1986b) were difficult to duplicate because the true significance of annealing procedure or surface cleanliness was not recognized. However, recent work concludes that Ne, Ar, Kr, and Xe moderators have comparative efficiency after proper annealing (Mills *et al.* 1994, Petkov *et al.* 1997, Jääskeläinen *et al.* 1997), with typical values for planar or simple conical geometry in the mid 10^{-4} to low 10^{-3} range. The absence of a pronounced correlation between energy gap and yields is consistent with suppression of epithermal e^+ neutralization at higher energies of the slowing down process because of the smaller positronium binding energy ($E_{\mathrm{Ps}} = E_{\mathrm{Mu}}/2$), and indicates a prominent role of energy dissipation via phonon excitation, which have similar energies in all RGS (see Table 1).

3.7 Temperature dependence and heat treatment of moderators

These data are especially useful to establish the relationship between emission and some structural and morphological properties of the cryogenic media (Morenzoni *et al.* 1997b). For the discussion we define a deposition temperature T_d, as the substrate temperature during deposition, and a moderator temperature T_m as the temperature at which the measurements are performed.

In Figure 16, the dependence on deposition temperature for Ar, Kr, and Xe moderators is plotted (in these cases $T_d = T_m$). For Ar and Kr, increasing the temperature first results in moderators that are superior to those deposited at the minimum temperature, but a further increase gives smaller efficiencies. For Ar a temperature of 15°K and for Kr a temperature of 30°K turns out to be optimal. For Xe no pronounced temperature dependence of the moderation efficiency is observed. It should be noted that, in all

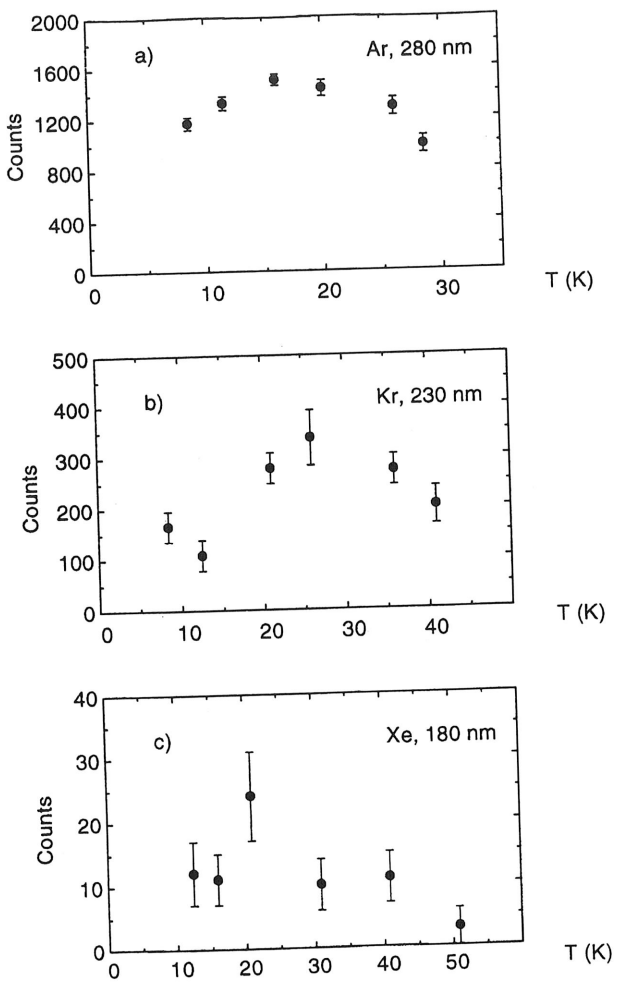

Figure 16. *Very slow μ^+ yield versus deposition temperature. (a) Ar, (b) Kr, (c) Xe.*

cases, at the highest investigated temperature noticeable sublimation sets in and the films become unstable. Since the very slow μ^+ emission in Ar and Kr depends on T_d it is interesting to investigate the effects of temperature cycling. In an experiment a fresh Ar or Kr layer was deposited at low temperature. Then the moderator was slowly warmed up to below the sublimation temperature. As shown in Figure 17 an effect can be observed. The warming up brings a continuous increase in yield of 20% in the case of Ar and of 50% in that of Kr, in agreement with the measured temperature dependence. By recooling the films to the lowest temperature the higher yields can be "frozen" and maintained, indicating that annealing produces some structural changes in the film. By contrast, N_2 shows no improvement upon annealing between 10°K and 20°K.

The experimental findings can be put in relation to the morphological and structural characteristics of the thin films of condensed gases, which are known to depend on the

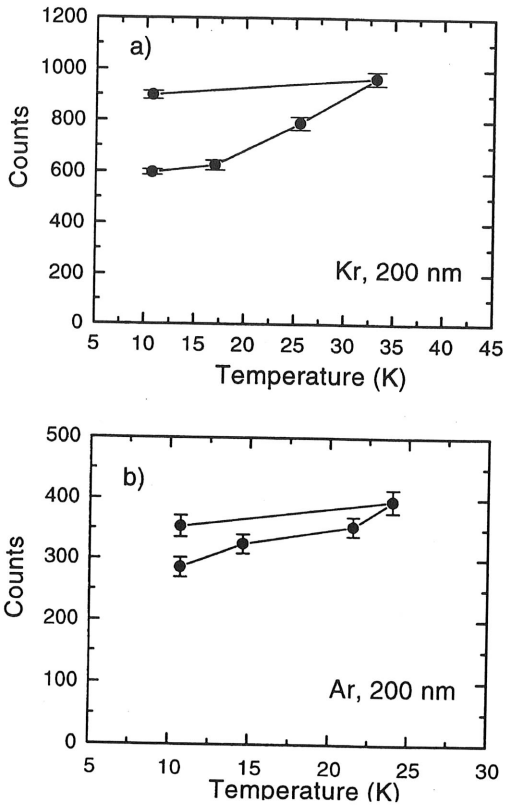

Figure 17. *Yields of epithermal muons during temperature cycling. The moderator is grown at the lowest temperature, then heated up slowly and finally recooled. (a): Kr, (b): Ar. The solid line indicates the temporal sequence in which the data are taken.*

growth conditions. Thin films grown from the vapour have polycrystalline structure. As for the bulk, crystallization of RGS occurs in face centered cubic lattices, but polycrystalline specimens contain more grain boundaries, defects, and voids and are generally more porous than when grown from the liquid. Films deposited at higher temperature just below the sublimation temperature have larger grain sizes and are less defective than films produced on a cold substrate, but the grain size in the substrate plane is generally limited to a few times the film thickness. If we compare these properties with our results, we may conclude that larger moderation efficiencies in Ar and Kr are correlated to higher degrees of crystallization (larger grain size, smaller number of defects). It seems, therefore, that the quality improvement of the thin film, which is achieved by increasing the temperature, is directly reflected in increased moderation efficiency. This is particularly evident from the annealing measurements. We can only speculate how grain size and defects influence the transport properties of epithermal μ^+ and their moderation. It is very improbable that defects and boundaries act as effective trapping sites of epithermal μ^+ . Presumably grain boundaries and associated defects introduce, due to the large polarizability of rare gas atoms, local dipole fields generating long range electrostatic potentials and thus

increasing the elastic scattering cross section and the nuclear energy loss per collision or providing an additional energy loss mechanism per collision. (Elastic scattering cross sections in the epithermal energy region are discussed in Section 4.) However, if grain size and defects were the only relevant parameters, we would expect a steady increase of the moderation efficiency with increasing T_d, in disagreement with the results for Ar and Kr. Other physical properties, which are temperature dependent, are the density and the morphology, which affect the porosity and the adsorption properties of the deposited film. It is known, *e.g.* from (Schulze and Kolb 1974), that the density of films of RGS and other van der Waals solids strongly depends on T_d. Moreover, at low T_d a maximum adsorption capacity has been observed, indicating an open-pore structure in this temperature range (Becker *et al.* 1972). The effect of open pores would consist primarily of enlarging the active surface area from which the epithermal μ^+ are emitted and hence of increasing the moderation efficiency. Also consistent with this interpretation are slightly increased yields for high deposition rates at a fixed temperature, since fast growing layers possess greater disorder and porosity. (The films are generally grown over a few minutes at a partial gas pressure in the 10^{-5}mbar range.) Reducing the density, further results in a diminished adsorption capacity indicating a closing of the porous structure. For the observed maximum of the efficiency versus deposition temperature we therefore propose as an explanation the interplay of two opposite effects, namely the competition between the efficiency increase due to the increase of grain size with temperature and the decrease due to the closing of the porous structure.

Again it is instructive to compare our results on μ^+ moderation in RGS with results on the most favorable growth conditions for e^+ moderators, where this question has been addressed only recently (Mills *et al.* 1994, Jääskeläinen *et al.* 1997, Petkov *et al.* 1997). Optimum efficiency has been reported for Ar at 16°K and Kr at 30°K, in good agreement with the μ^+ results. Proper annealing has a more pronounced effect for e^+ than for μ^+. The results suggest that the structural and morphological characteristics of the condensed layer have similar qualitative influences on both particles as far as transport is concerned. However, the granular structure and the presence of boundaries and associated defects have more pronounced effects on the delocalized e^+ than on the localized μ^+ . This causes the qualitative similarity in the temperature and annealing dependence and explains the more pronounced effects on the e^+ transport.

3.8 Surface adsorbates and decay properties

The long term stability of the moderator and the decay of the efficiency represent an important practical aspect for the development and use of a very slow μ^+ beam based on condensed gas moderators. Additionally, the understanding of these properties can also give insight into the processes governing the emission of epithermal μ^+ . The solidified film is submitted to the bombardment of energetic μ^+ and to the action of the adsorption of contaminants from the residual gas molecules. Both processes may produce a decay in time of the moderation properties, in one case by degrading or by eroding the layer, and in the other case by attenuating the probability that a very slow μ^+ created inside the moderator may be transmitted through the surface layer.

The influence of the residual gas is demonstrated in Figure 18 which shows the moderation efficiency of Ar as a function of time after layer deposition for three different

chamber pressures. At a pressure of 10^{-8}mbar the yield rapidly decays and no epithermal μ^+ are observed within a few hours. Ultrahigh vacuum conditions with pressures in the 10^{-10}mbar range are necessary and sufficient to maintain stable operating conditions over several days. This is also the case for N_2 and other moderators. It should be noted that UHV conditions are also necessary for most of the samples investigated by LE–μSR. The total pressure is a crucial but relatively rough parameter to characterize the complexity of possible mechanisms taking place in the adsorbate system formed by vacuum contaminants on the cryogenic surface. A detailed understanding of the specific role played by the different residual gas components (mainly hydrogen, water, CO and CO_2) is beyond the scope of this work. Nevertheless, some data have been obtained as a by-product of our studies. Neutrals and ions desorbed or sputtered by the projectile stem from the first monolayers of the moderator. Whereas the slow muon set-up is insensitive to neutrals, the ion species can be identified by our electrostatic transport system with the TOF measurement, which is sensitive to the mass to charge ratio.

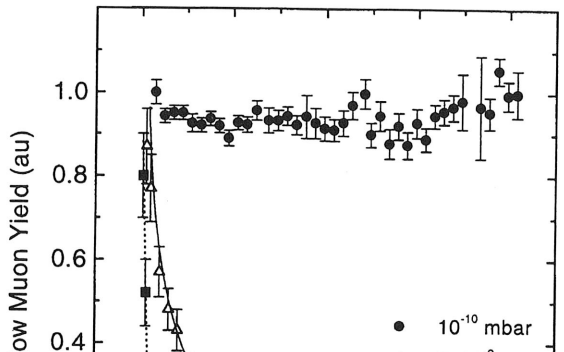

Figure 18. *Yields of very slow μ^+ from solid Ar as a function of time after layer deposition for different chamber pressures. (Yield normalized to value at deposition time.*

Time-of-flight spectra show, beside H^+, the presence of strong desorbing clusters from the surface of all RGS moderators consisting of a proton and n water molecules $(H_2O)_nH^+$, (protonated water clusters) (Figure 19). It is known that protonated water is the dominant cluster species emitted from pure water ice under ion and electron bombardment and that on foreign substrates water clustering occurs at coverages less than 10% of a monolayer. Therefore, the ion spectra observed may indicate the special role played by water molecules adsorbed on the surface in the decay properties of the van der Waals condensed gas films.

The ions represent only a small fraction of the ejected moderator material. Neutrals are much more intense and determine the amount of erosion experienced by the film. After traversing the moderator substrate, the surface muons have a wide energy distribution

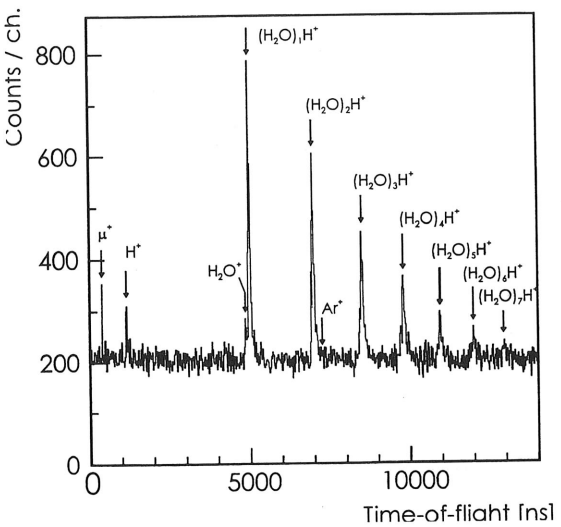

Figure 19. *Wide range time-of-flight spectrum showing ions and ion clusters emitted from a thin solid Ar layer. The spectrum is dominated by the protonated water clusters. The epithermal μ^+ peak is visible at short times.*

with a mean energy of 600keV. They typically deposit a few keV in the condensed gas film. Besides lattice damage, the interaction of the fast particles with the moderator produces desorption by the conversion of deposited electronic excitation energy into kinetic energy. This energy may initiate a cascade leading to the sputtering of atoms or molecules. For a possible use of condensed gas moderators at future very intense beams it is important to estimate the amount of erosion suffered by the moderator. We expect a similar sputtering behavior for muon and proton beams. Scaling proton sputtering data (Schou 1987), we conclude that, in the case of muon moderation, for Ar $\sim$0.4 atoms per incident fast muon, for N_2 $\sim$0.1 molecules/μ^+, and for Xe $\sim$0.02 atoms/μ^+ are ejected from the condensed gas layer. These numbers are too low to produce significant erosion of the solidified gas layer and to induce significant morphological degradation in the soft moderators. The decay properties are solely determined by the age of the layer, a fact also confirmed experimentally by switching off the beam and observing the time decay: no deviation from the behavior with beam on can be observed. A versatile use of the very slow μ^+ as magnetic microprobes of thin film samples requires that the moderator remains stable also in an adverse environment. Such a condition may be caused by intense thermal radiation originating from a hot sample. Measurement of the magnetization of thin Ni films as a function of temperature have shown that, even without special precautions, the cryogenic moderator remains unaffected at sample temperatures as high as 700°K.

4 Dynamics of epithermal muon generation/emission

The body of results collected up to now leads to the general picture of generation and emission of polarized epithermal muons as a consequence of hot μ^+-atom (or molecule)

processes inside the moderator. In this section, by amplifying arguments previously mentioned, we examine in detail the relevant mechanisms and interactions and quantify the corresponding cross sections. We address the question of how eV to keV muons interact with condensed matter and particularly with van der Waals insulators, why wide-band-gap insulators such as the ionic insulators do not possess pronounced moderator characteristics and discuss differences between atomic and molecular cryosolids. Finally, by considering the evolution of the muon transport during the moderation process, we interpret the experimental results in the framework of a hot diffusion process.

4.1 Outline of the basic physical model

The process of epithermal muon generation and emission can be regarded as composed of two essentially independent parts. In the first stage, energy lost by the incident energetic muons as a result of excitation and ionisation processes leads to the formation of an internal distribution of slow and very slow muons. These particles can be considered as the source of the epithermal muons. In the second stage, the so formed particles interact in various types of collision processes, where they lose only small amounts of energy. As a consequence, a fraction of the particles formed are able to reach the surface with sufficient energy and escape from the solid. Their properties are determined by the scattering, excitation, and reaction processes experienced by the muon on its way to the surface and by how it loses its last few 100eV of kinetic energy. Unfortunately, no experimental or theoretical information exists concerning this regime. We base our discussion mainly on data and theories that have been collected, respectively, developed for protons and hydrogen collisions with single atoms and molecules. To justify this procedure we have first to consider two issues: how can we link the behavior of particles in the solid phase to the better known behavior of particles scattered in the gas phase and how can we use available experimental proton data to quantify μ^+ interactions?

With respect to the first question the simplicity of van der Waals bound solids makes them a privileged system to study. Because of the small electronic coupling and of the weak interatomic and intermolecular binding, their fundamental electronic properties remain essentially unaffected upon condensation. To first approximation, they can be considered as dense gases and the influence of the surrounding atoms neglected. On the other hand, the wavelength of epithermal muons is short compared to the size of the atoms and, for the magnitude of the cross sections σ involved, the mean free path $\lambda = 1/N\sigma$ (N, atoms or molecules per cm^3) is much larger than the lattice dimension. Therefore, we begin by assuming that the fundamental properties of isolated scattering are valid also in the solid phase and discuss the interactions of the muons within a simple model of binary collisions where the muon excites mainly by direct interactions a collection of individual target atoms whose elastic and inelastic cross sections are essentially similar to those of a gas (Senba 1988). This also means that binding energy and vibrational motion of the atoms are neglected. A qualitative justification of this assumption may be obtained by considering the interplay of the interaction time between the μ^+ and the atom or molecule $\tau_{\text{int}} = a/v \sim 10^{-15}$s ($a$ lattice constant, v the velocity of the particle) and the characteristic period for lattice vibration $\tau_{\text{ph}} \approx 1/\omega \approx 10^{-13}$s (where $\hbar\omega$ is the characteristic phonon energy). From $\tau_{\text{int}} \ll \tau_{\text{ph}}$ it follows that the atoms can be considered initially at rest, that they recoil freely after a collision, and that the epithermal muons are too

fast to have noticeable interaction with phonons. It is clear that at very low energies the μ^+ may interact with the condensed medium in many body encounters, blurring the simple picture of strictly binary sequential collisions. However, the inclusion of many-body processes is not essential for the understanding of the fundamental properties of muon moderation and transport and there is no obvious way by which many-body effects should systematically modify the prediction of a binary collision picture.

The assumption that van der Waals bound solids essentially retain the properties of their individual atoms or molecules is also supported by experimental evidence. So, stopping powers of particles in gas and solid phase are similar. Electronic spectra of RGS are rather closely related to the free atomic spectra, though the energy levels may be shifted by 1–2eV to lower energies and the transition energies to higher energies. These electronic states are excited with the same magnitude in both phases. All these properties make possible links with gas-phase data. Similar characteristics hold true for the molecular cryosolids, where the covalent binding between the atoms in the molecule is much larger than the intramolecular cohesive energy of the solid and the weakly perturbed entities are molecules.

4.2 Collision processes, cross sections and energy transfer

The muon interacts in the moderating medium through inelastic collisions with electrons and elastic collisions with atoms. These processes can change energy, trajectory, and charge state of the μ^+. The most important inelastic processes to be considered for the positive and the neutral species are:

$$\begin{array}{lll} \mu^+ + A \rightarrow & \mu^+ + A^+ + e & \text{Ionisation by } \mu^+ \\ Mu + A \rightarrow & Mu + A^+ + e & \text{Ionisation by Mu} \\ \mu^+ + A \rightarrow & Mu + A^+ & \text{Muonium formation or} \\ & & \text{charge transfer or} \\ & & \text{electron capture.} \\ Mu + A \rightarrow & \mu^+ + A + e & \text{Electron loss.} \end{array} \tag{7}$$

Processes involving Mu^- can be neglected, because the cross sections are small. Molecular ion formation such as

$$\mu^+ + A + X \rightarrow \mu^+ + A + X$$

i.e. , muon attachment to molecules or atoms in "hot" collisions as well as the contribution of transfer of translational energy to vibrational and rotational degrees of freedoms in molecular van der Waals solids are briefly considered in Sections 4.6 and 4.7.

The threshold energies or energy defects of the various reaction channels are given in Table 2, together with the following parameters of van der Waals bound solids.

		Ne	Ar	Kr	Xe	N_2	O_2	CH_4
E_i	eV	21.559	15.755	13.996	12.127	15.58	12.08	12.51
E_g	eV	21.58	14.16	11.61	9.33	15.1		
E_{th}	eV	8.04	0.62	−1.93	−4.21	1.56	−1.46[a]	−1.03[a]
E_A	eV	−1.4	−0.4	0.3	0.5	−0.8		
U	meV	26.5	88.8	123.2	172.3	78	90	180
$\hbar\omega_p$	meV	6.4	8.0	6.2	5.5	8.3		10
N	10^{22}cm^3	4.54	2.67	2.22	2.73	2.21	2.28	2.7
Bond strength	eV	–	–	–	–	9.8	5.2	4.5[b])

Table 2. *Electronic properties, energies and physical parameters of van der Waals bound solids. (a) denotes a gas phase value and (b) a H-CH_3 bond.*

E_i	Ionisation energy of the atom or molecule
E_g	Band-gap energy in the solid (ionisation threshold)
E_{th}	Muonium formation threshold in solids (= E_g–13.539eV)
E_A	Electron affinity in the solid
U	Binding energy per atom or molecule
$\hbar\omega_p$	Largest acoustic phonon energy
N	Atoms or molecules per cm3

4.3 Energy transfer in inelastic collisions

To determine the magnitude of the inelastic collision processes it is plausible to assume that, at energies not too near to the threshold energy, cross sections for different projectiles are equal at the same relative velocity. The assumption allows to obtain the muon cross sections from the proton and hydrogen data from the relationship

$$\sigma_\mu(E_\mu) = \sigma_p(E_p) \qquad \text{when} \qquad E_p = (m_p/m_\mu)E_\mu. \tag{8}$$

This scaling law is based on velocity matching arguments between the atomic electrons of the target atom and the incident particle and reflects the cross section dependence on the interaction time, which is inversely proportional to the relative velocity. At energies of more than 100keV/nucleon, it finds its justification in the Born approximation. Our investigations of muon solid interactions (Prokscha *et al.* 1998) and first experiments with LE μ^+ presented in Section 6 confirm the scaling law down to muon kinetic energies of about one keV. (Simple arguments show that, at very low energies, the velocity scaling must fail. For instance, the ionisation cross section for proton on Ar is about $5\times10^{-18}\text{cm}^2$ at 100eV. If velocity scaling were still valid at this energy, μ^+ would have the same cross section at ~10eV. This is clearly impossible because conservation of energy requires a vanishing cross section for $E_\mu < E_g$. However, failure of the velocity scaling generally occurs in an energy regime, where the corresponding excitation process no longer plays a role in the slowing down and moderation processes.)

Figure 20 shows the ionisation cross sections or, more specifically, the cross sections for ejection of one or more electrons from the target obtained from a compilation by

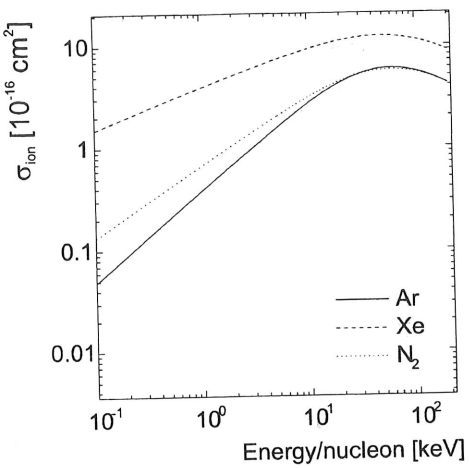

Figure 20. *Cross sections for ejection of electrons in Ar, N_2 and Xe as a function of the projectile energy per nucleon. The curves have been calculated from the recommended fits of Rudd et al. (1985).*

Rudd *et al.* (1985) as a function of energy per nucleon E/u where $m_\mu = 0.113u$. In the solid, this process corresponds to the creation of electron-hole pairs. The cross sections for Mu formation and electron loss calculated from analytical formulas derived by Nakai *et al.* (1987) are plotted in Figure 21. The figures provide an immediate indication of the magnitude of the cross sections of the electronic processes and their relative importance over a wide range of impact energies. Below some hundreds eV/u, the parametrisations show the correct trend. However, the absolute value may be uncertain since, in this energy region, no systematic measurements of these cross sections for proton projectiles exist because of experimental difficulties.

A comparison of the cross sections at low energies shows the pronounced effect played by the magnitude of the band-gap energy (or of the energy defect) on the size of the cross section. For instance, at 200eV/u, the cross section for Xe ionisation ($E_g \approx 9$eV) is more than an order of magnitude larger than the ionisation cross section of Ar or N_2 ($E_g \approx$15eV). Among the van der Waals solids, only Ne, Ar, and N_2 exhibit a positive threshold for Mu formation (Table 2). The energy required for this reaction has to be taken from the kinetic energy, thus putting a limitation on the energy range for which the process can proceed. For the other moderators the process is exothermic and can proceed without the need for an external energy supply. Figure 20 and 21 also demonstrate the fact that the influence of a positive threshold energy extends to much higher energies than the threshold itself. For instance at 30eV, Mu formation by capture of a Xe electron exceeds the Ar cross section by about a factor of 30. Concomitant with a smaller Mu formation cross section the elements where this process is endothermic exhibit a larger e^--loss cross section.

Knowing the cross sections, we can estimate the importance of the various collision processes in the different regimes of muon moderation. The transfer of energy associated with the reaction channels of Equation 8 results in a stopping cross section S, which can

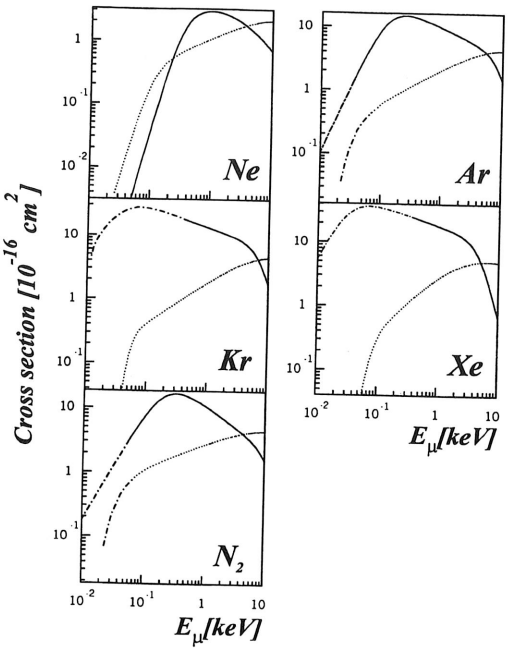

Figure 21. *Cross section for muonium formation and electron loss in Ne, Ar, Kr, Xe, and N_2 as a function of muon energy. Solid line: Mu formation. Dotted line: Electron loss. The curves have been calculated from the recommended fits of Nakai et al. (1987), by using the electron binding energies of the solid phase. Where the extrapolation to lower energies is more questionable, the general trend of the cross sections is indicated by a dash-dot line.*

be expressed by the cross section multiplied by the corresponding energy transfer E_i

$$S = -\frac{1}{N}\frac{dE}{dx} = \sum_i E_i \sigma_i = S_{\text{ion}} + S_{\text{CL}}, \tag{9}$$

where dE/dx is the energy loss per unit length.

At high velocities ($v \gg Zv_0$, $v_0 = \alpha c = c/137$, Bohr velocity), the electronic process which involves the largest transfer of energy is ionisation of the target

$$S_{\text{ion}} \cong \sigma_{\text{ion}}(E_g + \bar{E}_e), \tag{10}$$

where $\bar{E}_e$, the average energy of the ejected electrons, is roughly of the order of magnitude of E_g (Rudd *et al.* 1979). At lower energies, the frequency of electron capture events becomes comparable to that of ionisation events (this occurs in Ar at an energy of about 15keV) and electron capture and electron loss determine a charge changing cycle of the muon inside the moderator. For the calculation of the Mu formation and electron loss contributions we define an effective cross section

$$\sigma_{\text{CL}} = \frac{\sigma_{\text{Mu}}\sigma_{\text{L}}}{\sigma_{\text{Mu}} + \sigma_{\text{L}}}, \tag{11}$$

where σ_{Mu} is the Mu formation cross section and σ_{L} the electron loss cross section for the projectile. Equation 11 expresses the fact that the mean free path of the capture and loss (CL) cycle is equal to the sum of the mean free path of the individual processes. The energy lost in a cycle is given by

$$S_{\mathrm{CL}} = \frac{\sigma_{\mathrm{Mu}}\sigma_{\mathrm{L}}}{\sigma_{\mathrm{Mu}} + \sigma_{\mathrm{L}}}(E_g + E_{\mathrm{kin}}), \tag{12}$$

where $E_{\mathrm{kin}} = (m_e/m_\mu)E_\mu$ is the kinetic energy of the captured electron moving with the velocity of the muon.

Electronic processes involve the largest transfer of energy. According to Equations 10 and 12, an energy of the order of the band-gap energy of the moderator is lost in each ionizing collision or cycle. Since this energy corresponds to the average emission energy of epithermal μ^+, it is clear that the magnitude of the cross sections in the eV to a few hundreds eV range crucially determines the moderating properties of a given material. Because of its low, respectively, negative threshold, Mu formation is the most important inelastic process remaining effective when the μ^+ approaches the epithermal energy region. The μ^+ emerges from the charge exchange regime either as a positive muon or as muonium. The energy of last Mu formation can be approximated by the energy where the mean free path of the process is of the same order of magnitude as the escape depth of epithermal μ^+. We obtain for Ne, Ar, and N_2, which are the solids exhibiting the highest yields, following values 100±10eV, 10±5eV, and 10±5eV. Below this energy, the frequency of Mu formation is too low and the process is effectively deactivated. In the other moderators for which Mu formation is an exothermic process, electron capture, though suppressed, is not completely deactivated down to thermal energies. In these materials the cross section of the electron loss process is much smaller than that of Mu formation so that the probability of the muon ending up as epithermal Mu is very large and, correspondingly, the observed epithermal μ^+ yields are very low.

4.4 Energy transfer in elastic collisions

Elastic collisions with the atoms or molecules are the only energy loss mechanism available to epithermal muons falling below the energy of the last Mu formation. The elastic (also called nuclear) stopping cross section $S_n(E)$, can be written as

$$S_n = \int T \frac{d\sigma_{\mathrm{el}}}{d\Omega} d\Omega, \tag{13}$$

where T, determined by energy and momentum conservation, is the energy transferred in a collision with scattering angle θ, namely

$$T = \frac{4m_\mu m_{\mathrm{tgt}}}{(m_\mu + m_{\mathrm{tgt}})^2} E \sin^2 \frac{\theta}{2}. \tag{14}$$

Introducing the transport cross section

$$\sigma_{\mathrm{tr}} = \int \frac{d\sigma_{\mathrm{el}}}{d\Omega}(1 - \cos\theta) d\Omega,$$

and with $m_\mu \ll m_{\mathrm{tgt}}$, Equation 13 becomes

$$S_n \cong \frac{2m_\mu}{m_{\mathrm{tgt}}} E\sigma_{\mathrm{tr}} = \frac{2m_\mu}{m_{\mathrm{tgt}}} E\sigma_{\mathrm{el}}(1 - \langle\cos\theta\rangle), \tag{15}$$

where $\langle \cos\theta \rangle$ is the average of the angular distribution of elastically deflected muons and is a measure of the forwardness of the scattering process.

Equation 15 shows that more than the elastic cross section σ_{el} it is the magnitude of the transport cross section, which determines the energy loss rate. The transport cross section is an important quantity that permits to define the character of the particle motion. In case of isotropic scattering, where the direction of two consecutive paths is wholly uncorrelated and the muon migration is diffusion-like, $\langle \cos\theta \rangle = 0$ and we expect $\sigma_{el} = \sigma_{tr}$. However, a comparison in Figure 22 of the two cross sections for μ^+ + Ar collisions shows that down to the 10eV region forward scattering remains pronounced ($\langle \cos\theta \rangle \approx 1$). The anisotropy is a consequence of the atoms and molecules being much softer than a rigid sphere potential would indicate. The pronounced forward elastic scattering is confirmed by quantum mechanical calculations using a partial wave expansion technique of differential cross sections of very low energetic protons in solids, whose results are applicable to muons (Kawara and Ohya 1994). The forwardness of muon collisions at 10eV is in contrast to the behavior of positrons and electrons, dominated at this energy by s-wave scattering and where holds. As a consequence of the forward peaked elastic scattering, which reduces the effective magnitude of the elastic cross section by a factor of $1/(1 - \langle \cos\theta \rangle)$, and of the small ratio of the muon mass with respect to the target atom, elastic collisions are much less effective moderating mechanisms than electronic processes.

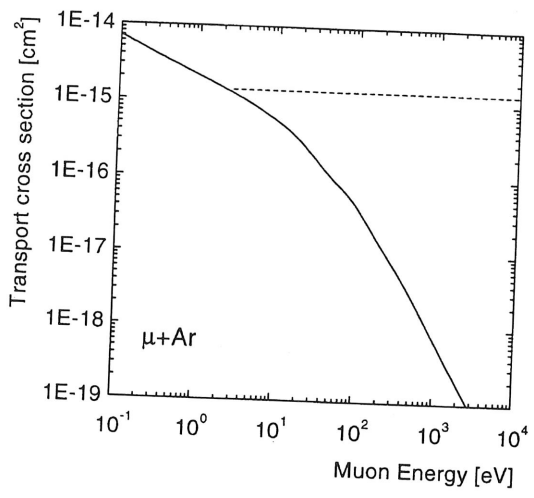

Figure 22. *Transport (solid line) and elastic (dashed line) cross for μ^+ -Ar collisions as a function of μ^+ kinetic energy; σ_{tr} has been calculated from the corresponding p+Ar cross section (Phelbs 1992); σ_{el} has been estimated from $\sigma_{el} \approx \pi p_{max}^2$ where p_{max} is the maximum impact parameter in the solid, determined from $p_{max} = (\frac{4}{3}\pi N)^{-1/3} = 0.6204 N^{-1/3}$. At very low energies this simple geometric approximation underestimates the importance of distant collisions and σ_{el} is expected to increase with decreasing energy.*

Summarizing, the closing of the endothermic Mu formation channel at epithermal energies ($E_\mu \geq$ 10eV) and the subsequent inefficient elastic energy loss mechanisms combine to make s-Ne, s-Ar, and s-N_2 the most efficient epithermal muon generators.

Also other van der Waals bound solids with weak exothermic Mu formation channel such as Kr, O_2, or CH_4 show relatively good moderation properties. In these cryosolids, the charge changing and elastic collision regime overlap down to very low energies. However, though energetically possible, Mu formation in the epithermal energy regime is sufficiently suppressed to allow an effective reduction of the energy loss rate and the formation and survival of a nonnegligible epithermal μ^+ fraction.

4.5 Processes in ionic insulators

The experimental findings on van der Waals solids lead to conclude that the muon state by the time it reaches the epithermal energy region depends primarily on the energy balance involved in the Mu formation. Large band-gap energy suppresses this and other electronic processes, a fact reflected in the moderation efficiency of RGS nicely correlating with E_g (see Table 1).

At this place the question arises why a very good insulator such as LiF with a band-gap energy approximately equal to that of Ar and N_2 exhibits a moderation efficiency which is about two order of magnitude lower. The understanding of this discrepant behavior is not only an interesting physical question but also has very important practical implications. It is evident that the availability of an efficient non-cryogenic moderator as a source of a low energetic μ^+ beam would offer more practical and user-friendly operating conditions than a condensed van der Waals gas. Unlike the RGSs, which have face centered cubic lattice with only acoustic phonons, alkali halides also support harder optical phonons. However, the contribution of optical excitation to the dissipation of muon energy is restricted by the weakness of the muon-phonon interaction and cannot explain the huge difference in μ^+ moderation efficiency.

The absence of moderating properties in LiF can be linked to the results of a recent measurement of the stopping cross sections of hydrogen projectiles with a few keV energy in this and other ionic insulators, where no influence of the band-gap energy on the velocity dependence of S was observed (Eder *et al.* 1997). An essential linear velocity dependence was found, similar to the case of metallic targets, where the dominant mechanism for slow particles to lose energy is electron-hole pair creation at the Fermi level, a process with no minimum energy transfer (Figure 23). This behavior is at variance with stopping cross sections in He and Ne gases, where the presence of a minimum excitation energy changes the linear velocity proportionality to a high power, between 2 and 4, of the velocity (Golser *et al.* 1991).

The unexpected findings can be explained by a mechanism of electron promotion as the relevant energy loss mechanism in ionic insulators at low velocity. As the muon and LiF complex begin to interact, they form quasi-molecular electronic states, which evolve from the atomic wave functions as projectile and target atom approach. A transition to an unoccupied state may take place, if the molecular orbitals (MO) for these states come sufficiently close together in energy for the states to be coupled. Molecular orbital promotion provides a mechanism to raise an electron from a bound level of the LiF crystal to an unoccupied state of smaller binding energy even by a rather distant soft collision (Figure 24). The formation of the molecular orbitals results in a significant local reduction of the LiF band-gap by about a factor of 2 with respect to the undisturbed crystal. This mechanism is also active at epithermal energies since the muon is attracted

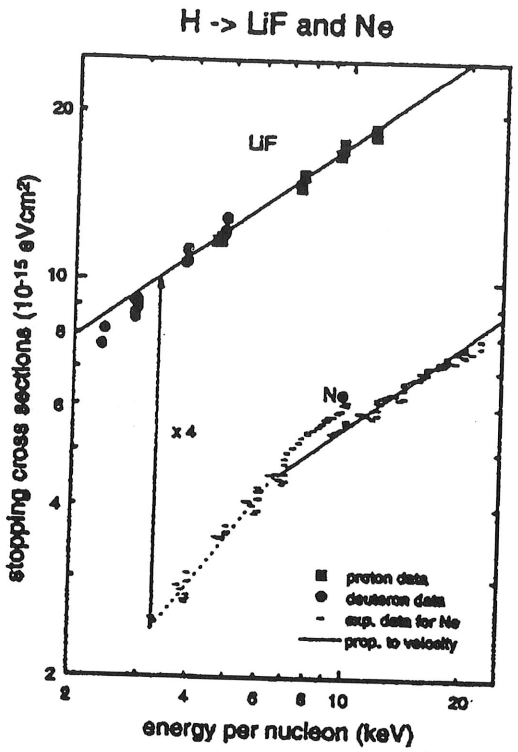

Figure 23. *Stopping cross section of LiF for protons and deuterons as a function of energy per nucleon. The stopping power is proportional to velocity as in a metal. For comparison the results for Ne showing the deviation from the linear velocity dependence are plotted (from Eder et al. 1997).*

by the negatively charged fluorine ion and MO formation between these two participants can occur quasi-adiabatically. Molecular orbital formation and coupling also enhance Mu formation through electron transfer from the fluorine ion to the μ^+. The lowering of the band-gap energy from 14eV to only 7eV and the large cross section for molecular orbital promotion introduce very effective electronic energy loss mechanisms, which make LiF a poor moderator. By analogy, we anticipate similar poor moderating properties for all alkali halides. Qualitatively another class of wide band-gap insulators as the oxides (SiO_2, Al2O3) should behave the same way due to the partial ionic character of their chemical bonds where the negative O ion plays the role of F^- in the fluoride.

The wave function overlap is rendered effective by the large ionic radius of the F^- centers of the LiF ionic crystal (0.136nm, atomic radius 0.05nm). We do not expect MO processes to represent epithermal energy loss mechanisms in the non-polar, closed shells van der Waals solids. Owing to the compact structure of a rare gas atom or of a N_2 molecule, the influence they exert on an approaching μ^+ is a short ranged one. It is strong only for small separation distances, which are not reachable at epithermal energies. The ionic character of the binding and the interstitial electronic distributions also affect the

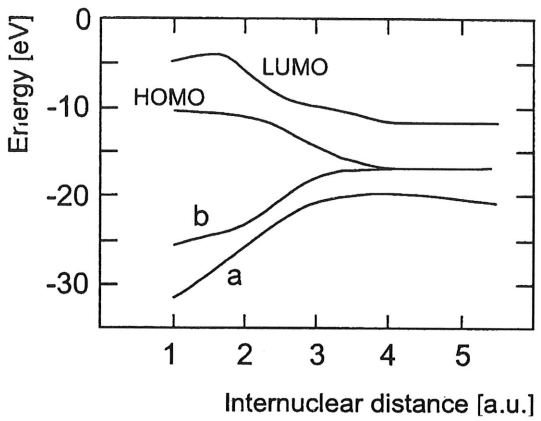

Figure 24. *Molecular orbital (MO) energy levels in the μ^+F^- system as a function of the distance between the two atoms R in atomic units (1 a.u.= 0.053nm). HOMO: highest occupied MO. LUMO: lowest unoccupied MO. The molecular orbital represented by (a) correlates at long interatomic distances with the 1s state of Mu, the curves labeled HOMO and (b) correlate asymptotically with the 2p orbital of F^-. The curves have been obtained from Eder et al. (1997).*

elastic muon-target interaction, which deviates from the interaction with neutral atoms. In molecules possessing a large permanent electric dipole moment and with no electrons or holes available to effectively screen the ionic charges, long range Coulomb forces act far beyond the nearest neighbors in the lattice. As a consequence, the elastic stopping cross section contains a significant second term which increases with decreasing energy resulting in an enhanced elastic energy loss cross section in the epithermal energy region (Biersack and Städele 1982). The long-range elastic interaction potential in ionic insulators combines with the mechanism of molecular orbital promotion to maintain sizable energy loss processes in the epithermal region. This leads to short mean free paths and small escape depths and is responsible for the very poor moderating characteristics of these and similar insulators.

4.6 Processes in molecular cryosolids: N_2

The understanding of the moderation in a molecular solid such as s–N_2 allows to test the model developed for the rare gas solids in a molecular wide-band-gap insulator, where additional degrees of freedom with corresponding excitation modes are possible. Molecules such as N_2, O_2, CH_4, ... have a rich vibration-rotation diagram. The transition energies and threshold energies involved in these excitation channels are much lower than those of electronic excitations and in principle the processes could be important down to thermal energies. Additionally, lower lying electronic excitation levels are present.

However, the comparison between Ar and Kr on one side and N_2 and O_2 or CH_4 on the other side displays a modest yield reduction in molecular cryocrystals with respect to atomic cryocrystals with similar band-gap energy. This indicates that projectiles like muons transfer little energy to excitation of bound states and very little energy into

vibrational, rotational, and librational motion. In this respect, it should be remarked that in the temperature range where the moderating thin film is stable N_2 (and O_2) solidify in the so-called phase, where the molecules are not free to rotate but are frozen along the diagonals of the fcc unit cell (in N_2) (transition temperature $T_{\alpha\beta}$= 35.6°K for N_2, and 23.6°K for O_2). Therefore, in this phase, interactions with the rotational modes are absent. Also other simple molecules such as CH_4 exhibit orientational ordering at low temperatures. Another interesting property making s–N_2 a good moderator is its triple bond which is one of the strongest bond known requiring an energy of ~10eV to break the molecule in two atoms (see Table 2).

The results confirm the picture outlined at the beginning of van der Waals bound solids as dense gases, with phonons not involved in the epithermal μ^+ formation and slowing down mechanisms. We conclude that the additional molecular excitation mechanisms do not play a major role in the epithermal moderation mechanism and that muons in a wide band-gap van der Waals solid have a behavior that is primarily independent of whether the solid is molecular or not. Therefore, we also expect relatively good moderating properties for other diatomic or polyatomic molecules with large ionisation gap such as CO and SF_6.

4.7 Muon transport

Up to now we have considered the mechanisms governing the moderation mainly from the point of view of energy transfer between muon and moderating particles, without taking into account the motion of the μ^+ in the moderator. It is clear that the most detailed description of moderation phenomena should include spatial and temporal aspects. In principle, the development in space and time of the initial forward peaked distribution of the energetic muons penetrating through the moderator can be formulated in terms of transport equations and described by a Boltzmann equation. Such a general statement of the problem needs, for a comprehensive treatment, a considerable amount of input, which is not available. For the present qualitative discussion, starting from the preceding energy considerations, we simplify the slowing down process in a good moderator in two energy regimes, roughly separated by the energy of the order of the last electronic process. In the first stage, the fast muons suffer energy loss but very little scattering and thus move in almost a straight line. At the moment of the last ionisation (several 100eV kinetic energy), the motion of the muon is still preferentially forward directed. This can also be deduced by considering the behavior of the relevant differential cross sections as well as from μSR experiments in van der Waals solids and liquids (He, N_2, Ar and Ne), where diamagnetic and muonium amplitudes of thermalized muons have been measured as a function of an external electric field (Krasnoperov *et al.* 1992, Storchak *et al.* 1997). These measurements allow to determine the relative muon-electron spatial distribution in the thermal stage. From the resulting non-isotropic distribution one concludes that the muons generally thermalise downstream from the center of mass of the electron distribution that has been ejected by them. It is interesting to remark that the characteristic muon-electron distance in α-N_2, about 50nm, is of the same order of magnitude as the escape depth of epithermal muons. Moreover, the existence of a sizable fraction of thermal muons well separated from the ionized electrons confirms the deactivation, at a later time, of Mu formation in the epithermal energy regime, in accordance with the discussion of Section 4.3. Following the suppression of the electronic excitation mechanisms and the onset of the soft elastic

collision regime, angular scattering becomes more important and the motion goes over into a transport of diffusive character. Finally, the stage of near to diffusion is reached, where the direction of motion becomes almost random.

It should be emphasized again that muon-atom elastic scattering at epithermal energies still is anisotropic. Nevertheless, as a consequence of the many soft elastic collisions the angular distribution of velocities evolves with time into an internal isotropic distribution, which gives rise to the observed external $\cos\theta$ distribution. This behavior can be expressed mathematically within a transport equation treatment and follows from $L \gg \lambda_{\mathrm{tr}} = 1/N\sigma_{\mathrm{tr}}$. Since in this stage the muon diffuses very rapidly loosing very little energy (hot diffusion), it is plausible to write a one-dimensional diffusion equation for the motion and emission of epithermal muons from a condensed gas layer:

$$D\Delta n(z,t) - \lambda_{\mathrm{abs}} n(z,t) = \frac{\partial}{\partial t} n(z,t) \tag{16}$$

where n is the density of epithermal muons at position z, D the diffusion constant, and is an absorption constant characterizing the rate of all loss and decay processes in the moderator. The major contribution to is the slowing down rate of "bare" μ^+ to an energy where escape is strongly suppressed.

By assuming the cryosolid layer-vacuum interface and layer-substrate interface to be absorbing, the flux of epithermal muons crossing the van der Waals solid surface at time t is given by

$$J(d,t) = -D \left.\frac{dn}{dz}\right|_{z=d} \tag{17}$$

. Moreover, since the thickness d of the frozen van der Waals film is much smaller than the μ^+ stopping width we can consider the initial density of epithermal muons inside the van der Waals layer to be homogenous, *i.e.* $n(z, t = 0) = N_\mu$ for $0 \leq z \leq d$ and $n(z) = 0$ otherwise. Solving the diffusion equation by standard methods and integrating over time, we obtain the stationary flux of epithermal muons :

$$j(d) = N_\mu \sqrt{\frac{D}{\lambda_{\mathrm{abs}}}} \tanh\left(\sqrt{\frac{\lambda_{\mathrm{abs}}}{D}}\frac{d}{2}\right). \tag{18}$$

If is normalized to the number of incoming fast muons, Equation 18 expresses the thickness dependence of the moderator efficiency. The two parameters λ_{abs} and D are related to the average escape depth L by

$$L = \sqrt{\frac{D}{\lambda_{\mathrm{abs}}}} \tag{19}$$

Equation 18 fits well the measured efficiency dependence on the thickness of the van der Waals bound solids and has been used in Section 3.5 to determine the escape depth. For sufficiently thick layers ($d \gg L$) and including a factor g that takes into account the geometry of non-planar moderator configurations Equation 18 becomes (ignoring the possible presence of a surface barrier and of reflection at the vacuum-moderator interface)

$$j = gN_\mu L. \tag{20}$$

This equation expresses the intuitive picture that the epithermal μ^+ yield is proportional to the epithermal muon density N_μ inside the van der Waals bound moderator times the

escape depth and a geometrical factor. For planar moderators g is equal to one, but it can be made larger than one, with consequent efficiency increase, by using an appropriate geometry (*e.g.* a structured surface, see Section 3.3, or a parallel array of foils). The parameter N_μ is given by the product of the epithermal particle density at the surface N_{stop} times the probability f_{epith} that the particles end up in the charged free state

$$N_\mu = f_{\text{epith}} N_{\text{stop}} \tag{21}$$

A Monte Carlo simulation shows that N_{stop} does not depend strongly on the moderator chosen and that for the experimental conditions used to obtain the results of Table 1 it amounts to typically 10^{-5} muons/nm. The fraction f_{epith} determined from Equation 20 using the experimental data summarized in Section 3 is shown in Table 3. The fraction distinctly departs from unity, providing direct evidence that not all particles reaching epithermal energies in the moderator are able to contribute to the epithermal μ^+ flux.

Moderator	f_{Mu}	f_μ	f_{epith}
Ne	0.07±0.05	0.93±0.05	na
Ar	0.74±0.04	0.26±0.04	0.17± 0.03
Kr	1.0±0.05	0.0±0.05	0.06±0.01
Xe	1.0±0.04	0.0±0.04	<0.006
N_2	0.84±0.04	0.16±0.04	0.2±0.05

Table 3. *Relative fractions normalized to one of thermalized Mu (f_{Mu}) and of diamagnetic μ^+ (f_μ) in the van der Waals gases (from Fleming et al. 1982) and epithermal μ^+ fraction (f_{epith}) in the solid phase.*

The values obtained are in good agreement with the diamagnetic thermal fraction $f_\mu \cong 1 - f_{Mu}$ in the corresponding low pressure (~2atm) gases, where Mu formation proceeds only via epithermal binary collisions and competing processes are absent. This result is an additional piece of evidence of the picture that Mu formation is the most important process competing with the generation of a source of epithermal μ^+ inside the condensed gas layer. It also supports the prediction, implicit in our physical model, of a prompt Mu fraction equal, to first approximation, in the gas and the solid phase.

Up to now we have not considered processes and mechanisms, which may be specific to the dense or solid phase. In the condensed phase, the picture of binary collisions between the muon and the constituents of the van der Waals bound solid must be extended to take into account processes between the muon and the product of a prior collision such as for instance its ionisation track. In addition, other processes, which may require a third body for stabilization, may play a role.

The question of relevance in the present discussion is whether and how these processes may affect the epithermal μ^+ formation inside the moderator. In solids and liquids, muonium can also be formed by delayed convergence of a thermalized muon with one of the electrons created in the μ^+ ionisation track (delayed Mu). Normally, even this process is complete before the usual μSR experiments begin, so that thermal and epithermal formation are not easily distinguished. The importance of the two mechanisms has been subject of long-standing discussions in the past. Recent experimental studies of electron mobility and Mu formation mechanisms in cryocrystals and cryoliquid (Storchak *et al.* 1997,

Brewer 1998, Storchak 1998) permit to make a distinction between prompt (epithermal) and delayed Mu formation on the basis of the time scale of muonium formation following implantation. This is obtained by observing the time evolution of the Mu polarization in external magnetic fields and by measuring the Mu and diamagnetic amplitudes as a function of external electric fields. From the experiments one infers that, in all the insulators investigated up to now, besides epithermally, Mu formation occurs via convergence of the thermalized μ^+ with a radiolytic electron and that the simple model taking into account epithermal processes and the convergence of the μ^+ with a track electron can explain the main features of the charge differentiation in the condensed van der Waals gases. These experiments indirectly confirm the presence of a sizable fraction of free epithermal μ^+ in the solid phase, since a large fraction (if not the totality) of the observed delayed Mu and diamagnetic signals (mainly due to molecular ions of the form $A\mu^+$, where A is a noble gas element or N_2) originates from epithermal μ^+.

In this respect, it is important to note the different observational time windows of the various experiments and the different time scale of the muonic processes. Whereas measurement of the μ^+ emission is directly sensitive to epithermal reaction channels, which take place for ps and represent a snapshot of the slowing down processes in the solid, measurements involving the motion of electrons toward the μ^+ focus on events occurring at a later time, following thermalisation and extending over a time scale of several ns. Therefore, the two types of experiments deliver complementary information. Globally, the μSR studies of cryosolids support the general picture of epithermal μ^+ emission, namely that only those μ^+ that primarily avoid epithermal Mu formation and are created within the escape depth contribute to the observed epithermal μ^+ yield. While the basic features of the epithermal μ^+ formation scenario are clear, some details need further investigations. For instance, the possibility of competing epithermal processes in the solid such as epithermal molecular ion formation, which may require a third body for stabilization should be further elucidated.

The present results give a new understanding of the dynamics of hot muons in solids. This is of relevance not only for the developments of LE–μ^+ science but insofar as the muon and its behavior in the moderator represent the case of hot heavy particle transport in solid. Moreover, this is of importance if one keeps in mind that even the dynamics of hot electrons in elements and compounds is still not well understood. A detailed understanding will rest on a better knowledge of the cross sections of the various elastic and inelastic collision processes, of the interactions of radiolysis products (primarily the electrons) with the muon, and of the dynamics of the μ^+ molecular ion complexes.

As far as the physical properties of the moderator are concerned, it appears that only atoms or simple molecules, belonging to the relatively narrow group of substances that are gaseous at room temperature and solid at low temperature, possess the necessary characteristics to gently slow down muons to epithermal energies. In these solids, the energy gap is large and the interatomic or intermolecular forces are weak and short ranged in their effect (but the intramolecular are strong). They differ from the other classes of solids in being made of discrete atoms and molecules. These characteristics introduce the necessary softness, that is reflected in the electronic and elastic interaction of eV particles with them and is in marked contrast to the dominance of strong, long-range Coulomb forces or electronic interactions in crystals possessing ionic character.

5 Low energy μ^+ as probes of thin films and surfaces

5.1 Overview of the low energy beam

Epithermal muons emitted from a moderator are the source of the low energy beam of polarized μ^+, which is the first example of a tertiary μ^+ beam. The first element of the beam is an acceleration section, which is inevitable because of the very short decay length of epithermal μ^+ (decay length $9\sqrt{E[\mathrm{eV}]}\mathrm{cm}$). The criteria for low energetic muon transport differ from those for other more readily available particles such as low energy electrons. Transmission is paramount and limiting apertures are avoided, as they would reduce the beam intensity significantly. The practical realization of the beam, which has been developed and is in use at PSI, is shown in Figure 6. The beam optics consists of purely electrostatic elements. Several "einzel" lenses and an electrostatic mirror are used to focus and deflect the very slow muons onto the sample. The mirror separates the slow μ^+ from the dominant fraction of non-moderated μ^+. These are not deflected appreciably by the electrostatic mirror and are detected in coincidence with the corresponding decay positron by a microchannel plate detector (MCP1), which is used for the optimization of the incident muon beam and for monitoring purposes. Characteristics of the tertiary beam such as intensity, source size and background level, depend strongly on the parameters of the surface μ^+ beam. The source divergency of the tertiary beam depends on the acceleration potential. Typical secondary beam spots cover a large area (depending on beam line and intensity between 2 and $30\mathrm{cm}^2$) and unless the size of the transport system is scaled up to dimensions colliding with cost and space limitations, transport without incurring in spherical aberrations or halo formation is not possible. The present system has been designed for a source size of $30\times30\mathrm{mm}^2$ corresponding to the beam size of the second most intense surface μ^+ beam at PSI (pE3). The beam spot at the sample position is circular with a radius of 7mm (FWHM). For the development and optimization of the LE–μ^+ beam detailed modeling, simulations and extensive beam mapping have been performed.

Between electrostatic mirror and sample, the transport section accommodates a retractable ultrathin detector, where a signal is generated by the passage of a slow muon. This detector (called trigger detector) is essential for time differential μSR measurements and other applications where a unique fast timing signal is needed. With pulsed beams (like those available at the synchrotrons at KEK or at the Rutherford Appleton Laboratory) such a signal can be obtained from the RF system of the accelerator or by detecting the muon bunch in a scintillator placed upstream of the moderator. The PSI cyclotron delivers continuous surface μ^+ beams. Since the yield of very slow muons per incoming fast muon is much smaller than unity, the scintillator detecting the incoming fast μ^+ cannot be used to provide an efficient start signal, unless an unacceptable reduction of the intensity of the incoming muon beam is taken into account. The problem has been solved by registering the moderated muons, pre-accelerated to typically 10–20keV, in a specially developed detector (Figure 25). It consists of a very thin carbon foil (thickness about 10–15nm, corresponding to about 50 to 70 atomic layers), combined with a MCP located perpendicularly to the foil. The μ^+ traversing the foil eject a few electron which are directed by a grid system to the MCP where they are detected. This scheme keeps the amount of material interacting with the muons and the consequent effects on the

trajectory minimal, while allowing for an efficient and fast detection. Still, the influence of the μ^+-foil interactions on the beam properties cannot be completely neglected. In the foil the μ^+ is scattered and loses energy. These processes are accompanied by a spreading of the energy (energy straggling) and possible neutralization, leading to some intensity loss—see Section 6. (It is interesting to note that this property could be used to produce a tunable low energy Mu beam.)

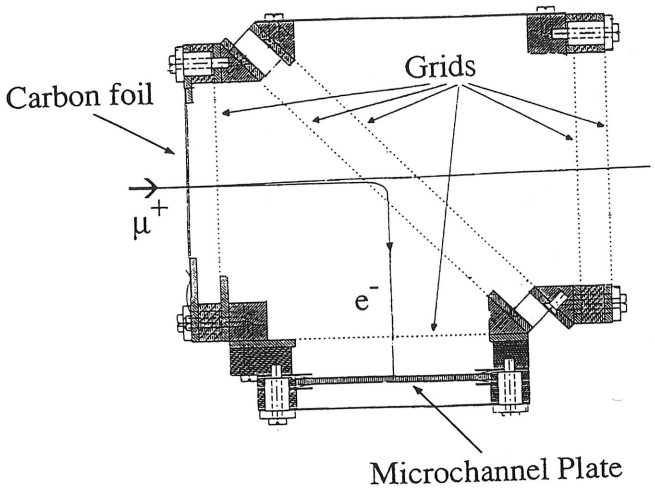

Figure 25. *Ultrathin foil detector for the detection of keV muons. Muons traversing the foil emit a few electrons, which are deflected by 90 degrees and detected by a MCP.*

At the sample position, Helmholtz coils generate a magnetic field of up to 0.3T parallel to the muon momentum and perpendicular to the spin. An iron yoke reduces stray fields. Whereas an axial magnetic field helps to guide the muon onto the sample, strong fields transverse to the muon momentum cannot be afforded. Samples can be mounted on a UHV cryostat or other holders allowing a temperature range between 5 and 800°K. The low energy of the μ^+ does not permit any window in front of the sample, which is directly connected to the vacuum chamber of the moderator. For a rapid change of the samples, a UHV gate valve separates the last section of the apparatus.

Energy range

The beam energy can be changed in different ways. The simplest method is to vary the extraction voltage of the moderator. However, two conditions limit the lowest energy that can be obtained by this method. The foil thickness of the trigger detector sets a lower limit of about 7keV. Below this value, energy loss, energy and angular straggling, and Mu formation in the carbon foil considerably degrade the quality and the intensity of the slow μ^+ beam. Even without the insertion of a trigger detector (possible at a pulsed accelerator), the μ^+ lifetime and the finite distance between moderator and sample sets a second lower limit of about 1keV. Biasing the whole trigger detector setup and accelerating the muons before they traverse the foil is a solution of the first problem.

The complete trigger detector including high voltage supplies and electronics is insulated from the rest of the apparatus and can be biased up to −30kV. In addition, biasing the sample in combination with deceleration (or acceleration) potentials in front of it permits a controlled reduction or increase of the kinetic energy by about 10keV, giving an implantation energy between 2keV and 30keV.

The most general scheme (in preparation), which allows to maintain the sample at ground potential, is the insertion of an acceleration-deceleration section between moderator and sample. For this, the part of the apparatus between moderator and sample, which includes the entire electrostatic transport system with trigger detector and related high voltage supplies and electronics, is electrically insulated and set to a high voltage of up to −30kV. This way, the moderated muons emitted from the condensed film are immediately accelerated to 30keV. In front of the sample, they return to their initial kinetic energy, which is determined by the extraction voltage and the energy loss in the carbon foil. This method offers largest flexibility for the sample environment combined with several collateral advantages. Since the muons, independently of the implantation energy, traverse the acceleration-deceleration section with equal energy the beam optics and other beam parameters need to be optimized for this fixed value only. Moreover, at 30keV, Mu formation in the trigger foil is negligible and the effects of multiple scattering and energy straggling are reduced.

Because the initial energy spread of the source is small, the energy width of the tertiary beam is determined by the energy straggling of the muons when they traverse the foil of the trigger detector (see Section 6.2 and Equation 24). This spread can be reduced by introducing, behind the foil, a cylindrical electrode with a time dependent potential that is pulsed by the signal of the trigger detector. One can program the shape of the time varying potential applied to the electrode so that the μ^+ exiting the foil with larger energy are decelerated by traversing the electrode and those exiting the foil with smaller energy are accelerated. This results in a convergence of the muons to a common point in energy. The degree of energy compression achievable will depend on how closely the ideal waveform can be realized. An improvement in energy resolution by a factor of 10 down to about 100eV seems realizable, since the necessary waveform parameters (average slope, delay time, voltage) are technically achievable.

LE beam intensity

The intensity depends on parameters such as moderator choice, secondary beam intensity and focal properties, background level, but also economic considerations. From the exclusive point of view of efficiency, s–Ne is the best moderator choice. It is the element providing the highest yields of very slow μ^+. Besides, the Mu fraction in this element is significantly lower than in other van der Waals gases (Table 3), suggesting an additional potential of improvement with respect to the figure of Table 1, which was not obtained under optimum growth conditions. However, the very low binding energy of Ne (see Table 2) requires for stable operation to keep the moderator cooled at temperatures near LHe temperature. Due to the large open area of the moderator, this can be obtained only with carefully designed and dedicated cryostat elements. In the existing LE–μ^+ set-up the less demanding s–N_2 and s–Ar moderators are routinely used.

Surface muon beam intensities at PSI range from 10^6 up to 10^8 μ^+/s (at 1.5 mA

proton current and $\Delta p/p \cong 0.05$). High intensity implicates a large acceptance beam at the primary production target with consequent large size of the tertiary beam source and accompanying higher background level. Therefore, emittance-acceptance matching criteria at the source of the LE beam and practical considerations such as reliability, stability and cost of the operation lead to the present preferential choice of the secondary beam line, which is characterized by intensities summarized in Table 4.

Surface μ^+ beam intensity	1.3×10^7/s
μ^+ incident on moderator	1.0×10^7/s
Epithermal μ^+ intensity at the source	380/s
Low energy μ^+ intensity at the sample	120/s

Table 4. *Present intensities of the spin polarized low energy beam at the $\pi E3$ beam line at PSI. Numbers refer to a proton current I_p=1.5mA, beam momentum p =27.5MeV/c, $\Delta p/p \cong 0.05$, N_2 moderator, and to the set-up shown in Figure 6.*

5.2 Interaction of low energy muons with solids and surfaces

LE muons, interaction with solids and surfaces In conventional μSR, generally, it is enough to know that the vast majority of the muons thermalise and remain well within the interior of the sample. By contrast, to fully exploit the potential of LE–μSR various aspects of the interaction of eV to keV muons in solids and surfaces such as implantation profiles, reemission or backscattering, and neutralization at the surface must be better understood. In complex systems (*e.g.* , multilayers), a precise knowledge of the depth distribution may be needed for a well-defined implantation in the sample and for the interpretation of the results. In other cases, it may be sufficient to characterize the distribution by the mean projected range R_p, the projection of the path of the particle along the normal to the sample surface, and the width of the distribution by the variance ΔR_p.

As for other aspects of LE muon science, this is an essentially unexplored field. The basic collision mechanisms involved are the same as in μ^+ moderation, but the transition from strong to weak energy loss mechanisms that makes possible the emission of epithermal muons from van der Waals bound solids may be disregarded in most implantation experiments. Neglecting diffusion, the implantation is governed primarily by the elastic and electronic energy loss in the energetic part of the slowing down process.

In practically all solids (excluding van der Waals bound solids), we expect that the total range is dominated by electronic stopping power. However, elastic processes are important in determining the scattering and hence the projected range, the straggling, and the depth profile. The relative importance of the two contributions depends on the velocity and is different in μ^+ and H^+ implantation processes. The rather scarce proton implantation data at very low energies cannot be simply scaled to obtain information about the corresponding muon behavior. Various analytical treatments of the transport of particles in matter are available but the variety of choices of atomic numbers and chemical composition of samples presents a difficulty for a comprehensive treatment. More realistic results are obtained by computer simulations based on Monte Carlo methods, where the slowing down and scattering of the projectile through the solid are followed step by step. These codes have had great success in modeling ion implantation distribu-

tions, for instance for semiconductor doping. A well known representative of this kind of approach is the program SRIM ("Stopping and Range of Ions in Matter") and its derivatives (Ziegler *et al.* 1985, Eckstein 1991), which can be used to calculate range distributions, backscattering, transmission coefficients and other collision parameters for any projectile/sample combination. These programs have been employed to quantify the implantation processes of μ^+ in matter (see Section 6). The use of LE–μ^+ for surface studies needs some additional considerations. To achieve direct surface sensitivity, softlanding of the μ^+ is necessary. However, at energies in the eV range, we expect that the muon does not penetrate into most of the samples and that reflection at the surface may take place. According to Thomas *et al.* (1992), the coefficient of reflection R_N of light particles (H^+, D+, T+ and He^+) obeys a general scaling relationship that depends only on a reduced energy variable ϵ ,

$$R_n = \frac{A_1 \ln(A_2\epsilon + 2.718)}{1 + A_3\epsilon^{A_4} + A_5\epsilon^{A_6}}, \tag{22}$$

where

$$\epsilon = \frac{32.53 m_{\rm tgt} E_\mu}{Z_{\rm tgt}(m_\mu + m_{\rm tgt})(1 + Z_{\rm tgt}^{0.23})} \cong \frac{32.53 E_\mu[\rm keV]}{Z_{\rm tgt}(1 + Z_{\rm tgt}^{0.23})}. \tag{23}$$

A set of fit parameters $A_1 \ldots A_6$ suffices to represent the data for $(m_{\rm tgt}/m_{pr}) > 20$. Figure 26 shows the energy dependence of the particle reflection coefficient. The reflection

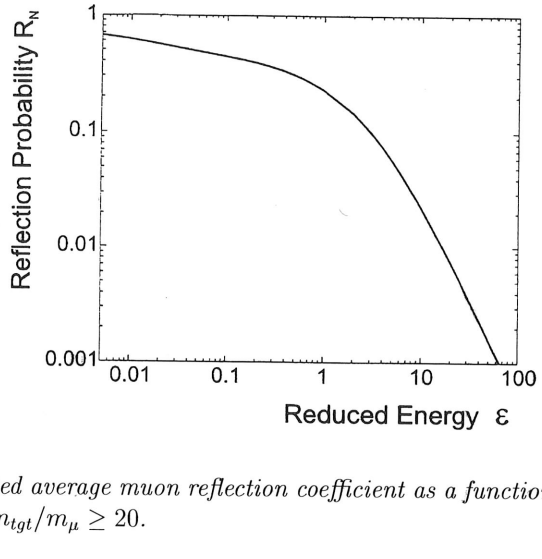

Figure 26. *Estimated average muon reflection coefficient as a function of reduced energy for the mass ratio* $(m_{tgt}/m_\mu \geq 20$.

probability increases with decreasing energy. Assuming Equation 22 to be valid for μ^+ we conclude that at very low energies reflection at the surface cannot be neglected. For instance at ~10eV about 60% of the μ^+ are reflected from a medium-mass sample. It should be noted that this number represents an average value. As with trapping, surface behavior of μ^+ is probably highly system-dependent and the final behavior of a very slow μ^+ impinging on a sample will be determined by the specific properties of the surface under investigation (composition, physical and chemical structure, morphology, presence of interstitials and defects, impurities, etc.). Simultaneous charge transfer in the interaction of muons with surfaces may also occur which could be used to study the electronic

and spin state properties of the surface of magnetic materials. We expect a higher neutralization at metal surfaces than at insulator surfaces, but detailed investigations are necessary in order to elucidate the behavior of epithermal μ^+ probes on surfaces. Besides softlanding of the particles, a possibility to obtain surface sensitivity might be to implant the muons at a sufficiently low energy ($E \cong 1$keV) and ensure that most of them rapidly diffuse back to the surface. Again, detailed investigations are necessary in order to assess the possibilities of this method.

6 First experiments with low energy muons

In this section, we briefly describe first experimental studies performed by using low energetic μ^+ and the LE–μSR technique. For an extended treatment of the different subjects, which encompass a wide spectrum of physical questions, we refer to forthcoming publications. Two experiments concern the field of muon-solid interactions and give basic information needed for the development of the LE–μSR method. In the other two experiments, LE–μ^+ were used for the first time as microscopic magnetic probes of thin film samples. Some of the presented results are of preliminary or exploratory nature and the main intention of this section is to illustrate potential applications of the new technique in different fields of muon science. (The experiments reported here have been performed with a LE–μ^+ flux at the sample of about $40\mu^+$/s.)

6.1 Measurement of μ^+ implantation profiles by LE–μSR

In many experiments, ranges and other implantation parameters used as input to data analysis have to be obtained by simulation. Therefore, before using LE–μ^+ for depth resolved μSR, it is of the utmost importance to asses the reliability of the predictions obtained from Monte Carlo codes, which may differ quite appreciably. Generally, there are some difficulties in analyzing and measuring ranges of keV implants. Depth profile experiments with protons and other stable ions have to face the difficulty that the position where the particle comes to rest must be determined in a separate experiment. The muon as a light proton, decaying with unique signature and precessing with frequencies depending on the local magnetic or electronic environment, offers, in combination with LE–μSR techniques, the possibility to investigate implantation processes by a completely new approach. The study of implantation profiles of low energy muons in matter is not only a necessary prerequisite for their use in thin film investigations but represents a novel test of our understanding of the implantation of heavy particles in matter, a field with a wide range of technological implications.

To determine the stopping site of a muon we rely on the property that muons thermalized in metals remain in the diamagnetic state, whereas the large majority of muons thermalized in insulators and semiconductors form Mu, which has a hundred times a larger Larmor frequency. In a sample composed of two or more materials where the muon shows a different behavior, the implantation profile can be studied by measuring the precession frequency in an external transverse magnetic field as a function of energy and of the thickness of the individual layers. In principle, other known material dependent parameters such as asymmetry and relaxation could also be used for these studies and in

magnetic materials the precession frequency in zero field could be taken as a signature of the muon site. As an example of the method, Figure 27 shows a result from an experiment where μ^+ with different energies have been implanted in Cu/SiO_2 samples (Cu layer of thickness between 0 and 150nm, sputtered on a very pure SiO_2 substrate). The measured fraction of μ^+ stopped in a 50nm Cu layer is compared with the prediction of a Monte Carlo computation (TRIM.SP code, Eckstein 1991). This program extending the range of applicability of the well known SRIM code (Ziegler *et al.* 1985) to smaller energies and allowing a better handling of the transport through interfaces well reproduces the experimental data. Comparisons between experimental data on R_p and ΔR_p of few keV protons in light elements with different simulations (Mayer *et al.* 1994) have also given good agreement with the predictions of this program. The results indicate that the basis of this code (interaction potential, inelastic energy loss contribution and other sample parameters) can be used to obtain reliable estimates of μ^+ depth profiles in matter.

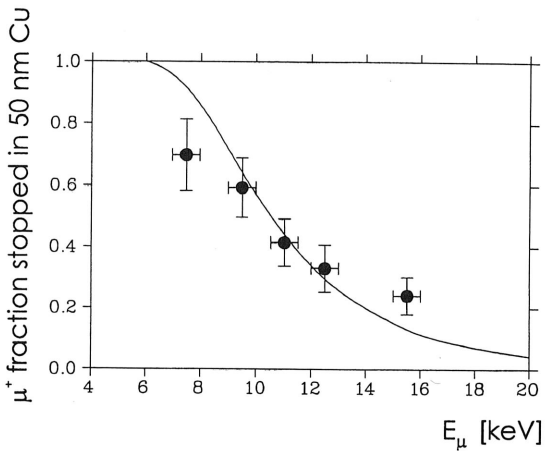

Figure 27. *Fraction of μ^+ stopping in a 50nm Cu film on a SiO_2 substrate as a function of the implantation energy. The curve represents the prediction of the program TRIM.SP (Eckstein 1991).*

We used this program to simulate the implantation profile of μ^+ in some samples. Figure 28 presents for example the depth profile of μ^+ with energies in the range between 1keV and 18keV in the high-Tc superconductor $YBa_2Cu_3O_7$. The distributions have a typical relatively broad maximum and a tail to lower depths. As an indication of the material and energy dependence of the implantation parameters, Figure 29 shows the results for R_p and ΔR_p as a function of the μ^+ implantation energy in a low (SiO_2), a medium (Ni), and a high (Au) density (and Z) element. At fixed energy, decreasing Z increases the mean penetration depth and narrows the relative width of the distribution. The figure illustrates the fact that μ^+ with energies between ~10eV and ~20keV cover in optimum way implantation depths ranging from the subnanometer to the 100nm region. Protons with the same energy penetrate deeper than muons and have larger depth distribution. For instance, at an energy of 1keV the simulation yields R_p =7.1nm and ΔR_p = 3.5nm for μ^+, and R_p =12.6nm and ΔR_p = 6.4nm for protons. The smaller μ^+ penetration depth is a consequence of the larger μ^+ electronic stopping power, which is proportional

to the velocity in this energy range. It should be noted that diffusion and trapping of the μ^+ after thermalisation might noticeably modify the stop distribution as determined by electronic and elastic processes. Therefore, depending on the sample characteristics and experimental parameters, the thermal interactions might be also considered to determine the effective μ^+ site distribution when they decay.

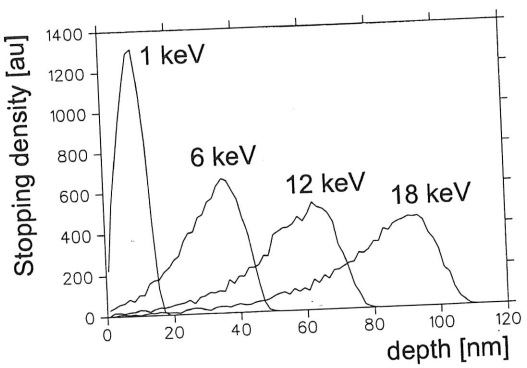

Figure 28. *Simulated implantation profiles of μ^+ in YBCO as a function of energy.*

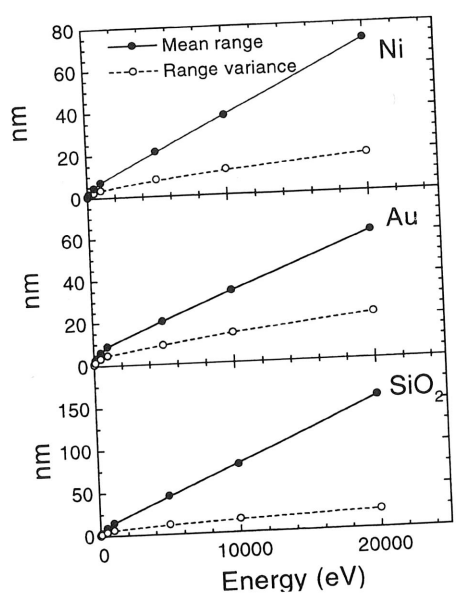

Figure 29. *Calculated energy dependence of the mean projected range and of the variance of the depth distribution of μ^+ in Ni, Au and SiO_2 samples.*

6.2 Muon-solid collision processes

We have measured the energy dependence of stopping power, energy loss straggling, and charge neutralization of muons traversing a few nm thick carbon foil. Since the beginning, the problem of energy loss of ions moving through solids has attracted the attention of physicists such as Bohr, Bethe, and Bloch and is still subject of intense investigations. Until now, studies with μ^+ have been hampered by the lack of availability of monoenergetic muon beams and the presented experiment represents the first direct measurement of these quantities. The experiments are an example of applications of LE–μ^+ to the physics of atomic collisions whose theoretical importance resides in the fact that it represents a wide benchmark for approaches to processes in a case where the force producing the transition is well known. A better understanding of stopping powers and related quantities is also of great practical importance for the interpretation of a variety of experiments and techniques (ranging from ion-beam analysis, implantation in material science and technology, to the use of protons and heavy ions in radiotherapy) and for the understanding of the physics of muon moderation. Specifically, the present experiment was motivated by the need to quantify the interaction of keV μ^+ with a thin carbon foil, which is an essential part of the LE–μSR set-up

Theoretically, one expects that at not too low energies the cross sections of collision processes depend on the velocity of the projectile but not on its mass. Up to now, this velocity scaling has been tested by using protons and other heavy ions as projectiles. However, the comparison is complicated by the fact that in a heavy ion the complex many-electron structure leads to a variety of excitation processes that somewhat obscure the details of the elementary collision processes. The muon is an ideal projectile to test theoretical models, since it offers the simplicity of a heavy projectile with unit charge, such as the proton, but with a mass intermediate between proton and electron.

For the measurements, we use the thin carbon foil of the trigger detector (described in Section 5) as a target, and the experimental set-up of Figure 6 with MCP2 installed at the sample position. The exit energy spectrum as well as the charge state distribution as a function of the incoming muon energy is obtained from the TOF information between the two detectors (Figure 30). A particularity of the experiment is that the behavior of equi-energy protons is measured simultaneously. This is due to the fact that some atomic or molecular hydrogen is always present as a residual gas component in the UHV apparatus. Hydrogen, free or bound to molecules and sticking on the moderator surface, can be ionized by fast muons, acquire the same energy and follow the same trajectory as the extracted epithermal muons. This peculiarity, eliminating sources of systematic error, makes the measurements inherently very accurate and permits to obtain a direct test of velocity scaling. In the TOF distribution of the μ^+ and p a double peak structure is visible. The most intense component corresponds to the slow μ^+ (and p), which have lost some energy after traversing the foil. The other component is produced by those slow μ^+ and p, which capture an electron in the foil and continue as muonium or hydrogen, respectively.

The measured charge state yields of muons and protons passing carbon are plotted in Figure 31 as a function of the residual energy per mass unit E_{out}/u , which depends only on the exit velocity. It should be noted that the UHV conditions of the LE–μ^+ apparatus offer an additional benefit for this type of measurements, since they reduce

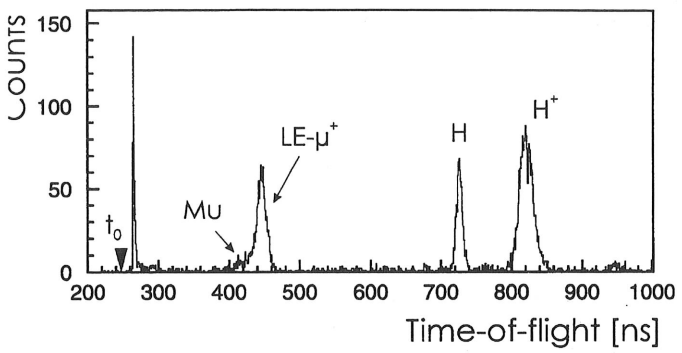

Figure 30. *Time-of-flight distributions of muons and protons after traversing a thin carbon foil with 15keV incident energy. The neutral and the charge states are visible.*

possible spurious effects arising from adsorbed layers on the C foil surface. Figure 31 shows that, with decreasing energy, the neutral fraction increases and reaches almost 100% at very low velocities. The full lines are the prediction of a charge exchange model for hydrogen projectiles (Gonin *et al.* 1994), where the distribution of the outgoing particles is determined by charge exchange inside the solid and by electron tunneling between the carbon surface and the exiting particle near the surface outside the solid. The Figure shows that the muon and hydrogen data can be predicted within a relatively simple model and that the charge yields depend only on the exit velocity.

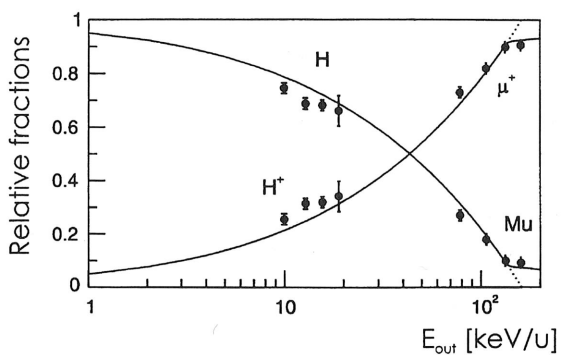

Figure 31. *Charge states of muons and protons passing carbon. The full lines are predictions of a model including charge exchange by dynamic screening inside the solid and tunneling at the surface.*

Also the data about energy loss and energy loss straggling can be well described by velocity scaled empirical formulas which have been recently compiled for protons from available theoretical and experimental material (Berger *et al.* 1993, Yang *et al.* 1991, Hofer 1998). From the measurements, we infer that the typical energy loss of LE–μ^+ traversing the trigger detector foil is about 2keV with an energy straggling of about 500eV. In the energy range of interest for LE–μSR applications, the straggling Ω can be expressed by a simple formula derived by Bohr (1948) that is independent of the projectile velocity and

of the electron distribution in velocity and space and that is valid for $v_{\rm pr}^2 \gg Z_{\rm tgt} v_0^2$,

$$\Omega^2 = 4\pi Z_{\rm pr}^2 Z_{\rm tgt} e^4 N d \tag{24}$$

with d the thickness of the foil.

In conclusion, the first measurements of energy loss, energy loss straggling, and charge yields of low energetic muons show a good agreement with velocity scaled proton data. These measurements demonstrate that the LE–μ^+ beam, besides its main application in LE–μSR spectroscopy, can be used as a new experimental tool for the study of particle-solid interactions. There is an interest in extending the present measurements to other metallic and non-metallic targets and to lower muon velocities where projectile mass effects and deviations from velocity scaling can be expected. Of particular relevance for the physics of μ^+ moderation and transport of eV particles in solid would be measurements of excitation processes at low and very low velocities in van der Waals solids and other insulators to study the deactivation of electronic processes in these solids.

6.3 Investigations of high-Tc superconducting films

A technique such as μSR, which measures magnetic fields and their fluctuations at local points of the sample lattice, can provide detailed information on the superconducting state in various materials that complement macroscopic magnetization measurements. In the last decade, special attention have received the new high-temperature (HTC) superconducting oxides. In these type II superconductors, in an external field in the range $B_{c1} < B_{\rm ext} < B_{c2}$, the magnetic flux $\mathbf{B}(\mathbf{r})$ varies spatially since it penetrates in form of a (more or less regular) lattice of flux lines (tiny current vortices) each carrying one elementary flux quantum $\Phi_0 = h/2e = 2.07 \times 10^{-15}\mathrm{Tm}^2$. These vortices have a core of radius $\sim \xi$ (coherence length), within which the superconducting order parameter goes to zero, and carry a flux tube of radius $\sim \lambda$ (magnetic penetration depth for weak magnetic fields). The μSR method has proved to be able to provide a measure of the microscopic flux distribution $\mathbf{B}(\mathbf{r})$ inside the bulk of samples, to yield information on the dynamics of the vortex state (Herlach *et al.*, 1990, Keller 1990, Aegerter and Lee 1997, Lee 1998), and has been used to characterize and classify superconducting materials (Uemura 1991, 1998). The vortex state of a type-II superconductor produces a distinctive μSR line shape (distribution in frequency domain) with features determined by the average internal field $\langle B \rangle$, by the characteristics lengths λ and ξ, and by the degree of disorder in the vortex lattice. Also phenomena such as flux-line pinning, flux-line melting and flux-line motion, which have technical relevance when preparing materials that must operate under high magnetic fields in devices without dissipation losses, have been subject of several studies (Lee *et al.* 1993).

During the last few years, it has become clear that many of the applications most likely to be realized (conductors for magnets or for power transmission, RF devices, etc.) will be based on thin films. Moreover, well characterized thin films are a privileged object of investigation to understand the essential characteristics of HTC superconductors and a significant effort has been put into the realization of epitaxial films of oxide materials as well as in the study of the influence of the growth parameters on the physical properties of these materials. YBCO ($YBa_2Cu_3O_7$) is one of the central compounds and seems to be one of the materials of choice for applications. It is possible to fabricate even double-sided

high quality homogenous films on substrate areas up to more than 20cm diameter (Utz *et al.* 1997).

With LE–μ^+ we investigated for the first time films of $YBa_2Cu_3O_{7-\delta}$ with the purpose to test the present potential of LE–μSR for studying microscopic properties in thin HTC samples. The first sample consisted of a high quality 500nm thick, epitaxial $YBa_2Cu_3O_{7-\delta}$ film ($\delta \approx 0$) grown by reactive thermal coevaporation on a $LaAlO_3$ substrate using a method described in Berberich *et al.* (1994) (Kinder 1997). The experiment was performed in the transverse field set-up with the crystallographic c-axis parallel to the shortest dimension and to the external magnetic field. The critical temperature as determined by magnetization measurements was T_c =87.5°K .

The μSR technique allows a direct measurement of the local magnetic field probability distribution $p(B)$ in the superconductor, which is related to $P(t)$, the time evolution of the muon polarization along the axis perpendicular to the applied field, by a simple relationship

$$P(t) = \frac{1}{V} \int_V \cos\left[\gamma_\mu B(\mathbf{r})t + \Phi\right] \, d\mathbf{r}, \tag{25}$$

where V is the volume of the sample and Φ the initial phase of the muon spin.

This equation can be written as a Fourier transform

$$P(t) = \int p(B) \cos\left[\gamma_\mu B(\mathbf{r})t + \Phi\right] \, dB, \tag{26}$$

where the function $p(B)dB$ (called line shape) represents the internal field distribution, *i.e.* the fraction of the sample which has a local field with magnitude between B and $B + \delta B$.

Figure 32 shows the time decay spectra measured at different temperatures with the sample cooled in a field of B_{ext} = 28mT. In these measurements the low energy muons were implanted into the sample at a kinetic energy of 16keV corresponding to an implantation profile with mean penetration depth of 71nm and FWHM of 25nm. The increasing damping of the precession signal with decreasing temperature reflects the broadening of the internal field distribution due to the formation of a flux line lattice. The line shape may be extracted from the measured asymmetry spectra via a Fourier transform using a so-called maximum entropy technique (Rainford and Daniel 1994). This technique is more effective for Fourier analysis than the more common fast Fourier transform, since it reduces the effect of Poisson noise in decay spectra with low statistics. Figure 33 shows $p(B)$ at different temperatures after subtraction of the contribution to the spectrum from muons not stopping in the sample. At 100° K, above the critical temperature, the external field is detected. By lowering the temperature below T_c, the distinctive asymmetric line shape develops.

The broad asymmetric shape with a maximum at a field B_{saddle} lower than B_{ext} shows features characteristics of a vortex-line lattice structure including the long tail towards high fields, which corresponds to regions of the lattice close to the vortex core (Lee 1998). The field with maximum intensity corresponds to the saddle point between two vortices, which in an ideal vortex lattice appears as a cusp below the average field. In the field region considered here, $p(B)$ is determined primarily by the London penetration depth and the geometry of the vortex lattice. The data have been fitted to an internal field distribution according to the London model plus a Gaussian background distribution. In

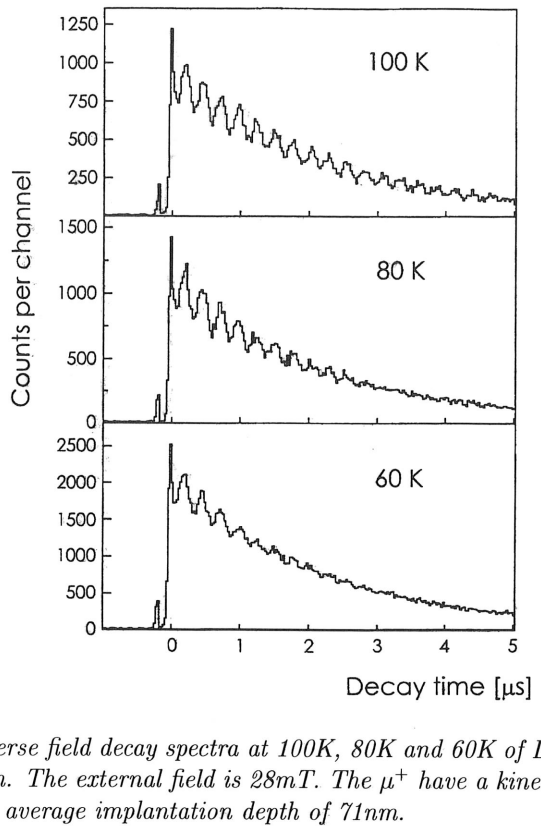

Figure 32. *Transverse field decay spectra at 100K, 80K and 60K of LE–μ^+ implanted in a 500nm YBCO film. The external field is 28mT. The μ^+ have a kinetic energy of 16keV corresponding to an average implantation depth of 71nm.*

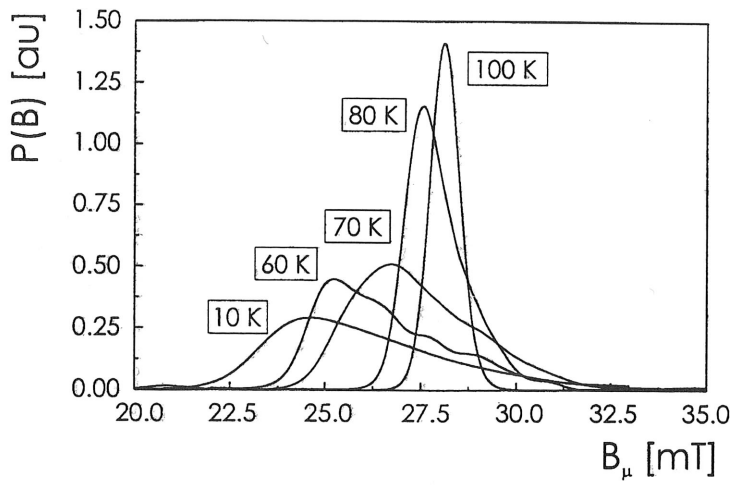

Figure 33. *Probability distributions of the internal magnetic fields in YBCO (500nm) at different temperatures measured by low energy μ^+ at $B_{ext} = 28mT$.*

the model, the local field at $\mathbf{r}$ is a simple superposition of the fields from the separate vortices arranged in the triangular Abrikosov lattice (Abrikosov 1957) with intervortex spacing a given by

$$a = \sqrt{\frac{2\Phi_0}{\sqrt{3}B_{\text{ext}}}} = \frac{1546\text{nm}}{\sqrt{B_{\text{ext}}[\text{mT}]}} \tag{27}$$

The isotropic London model is appropriate since $\xi \ll \lambda$, $\xi \ll a$, and the field is applied along the symmetry axis of the superconductor; λ refers to the magnetic penetration depth in the copper oxide planes (λ_{ab}) and is directly related to the number density and effective mass of the superconducting charge carriers. From the fit, a magnetic penetration depth $\lambda_{ab}(60K) \cong 185\text{nm}$ is obtained. The fit includes a convolution with a Gaussian distribution of fields to take into account deviations of the flux line lattice from a triangular array (due to random vortex pinning, flux line distortions, thermal fluctuations, etc.) (E. Brandt 1988) and instrumental resolution, The measured line shapes in thin films are similar to the results obtained with bulk samples, where μSR measurements are generally performed in the regime characterized by $\lambda > a$. These measurements in a thin film at 28mT and similar results at 5.3mT indicate that long range order over distances of the order of the vortex distance also persists in the low vortex density regime, where the vortex fields do not overlap and the mutual interaction is strongly reduced. Fluctuations in spacing of the vortex lines must be much smaller than a, since fluctuations on a scale of a would result in a symmetric line shape.

From the variation of the line shape with temperature the temperature dependence of the magnetic penetration depth $\lambda(T)$ can be determined: for an ordered triangular flux line lattice the position of the saddle point is related to the London penetration depth by:

$$\langle B \rangle - B_{\text{saddle}} = 0.0368 \frac{\Phi_0}{\lambda^2}. \tag{28}$$

For the sample and field geometries used in the experiment $\langle B \rangle = B_{\text{ext}}$. Figure 34 shows the results obtained from the magnetic field distribution measurements at 28mT. The solid curve represents a fit to a power law of the form

$$\lambda(T) = \lambda(0) \left\{1 - (T/T_c)^n\right\}^{-1/2}. \tag{29}$$

For the investigated film $\lambda(0) = 146 \pm 10\text{nm}$ and $n = 2.2 \pm 0.4$. The value at T=60°K is in good agreement with the value obtained from the line shape analysis. The functional dependence and the value for $\lambda(0)$ are consistent with results from a conventional μSR experiment in a single crystal $YBa_2Cu_3O_{6.95}$, which finds $\lambda(10K) = 149 \pm 2\text{nm}$ and $n = 2.89 \pm 0.23$ (Riseman *et al.* 1995). Other measurements of different specimens also yield values in the range $\lambda(0) \cong 140$–150nm (Fuchs *et al.* 1996). A fit with $n = 4$ (two-fluid model) also shown in the figure, and which is usually well supported by experiments on conventional superconductors, is not able to predict the observed temperature dependence.

In another series of measurements, the variation of the magnetic field distribution in the vortex state above and below the surface of the superconductor could be measured by varying the implantation energy of the LE–μ_+. Calculations within the London model predict that the field distribution inside a thin film of a type-II superconductor, with external field perpendicular to the surface, is bulk like at a distance $z \approx a$ below the surface (Long and Forgan 1997). Approaching the surface, below $z \approx 0.2a$, B_{saddle} shifts

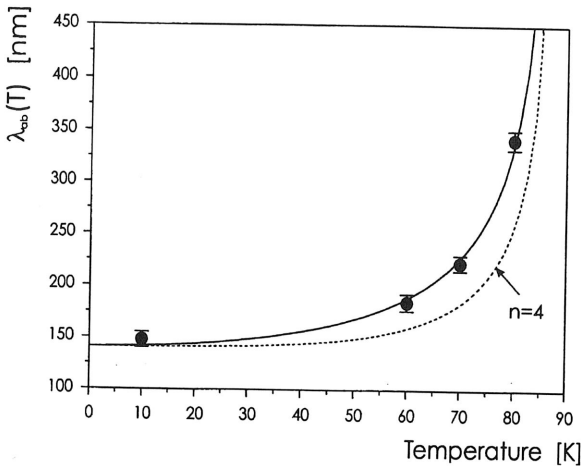

Figure 34. *Temperature dependence of the magnetic penetration depth for a thin YBa2Cu3O7 film recorded in a field of 28mT. The solid line is a fit to $\lambda(T)$ of Equation 29. The dotted line is a fit to BCS s-wave theory with n=4.*

significantly towards B_{ext} and the width of the distribution diminishes. Above the surface at a distance of about $-0.1a$ the distribution is still asymmetric but the high field cutoff noticeably moves to lower values. At $z \approx -a$, the field becomes homogenous and equal to B_{ext} .

We have tested this behavior by implanting LE–μ^+ at different energies in YBCO. Besides the 500nm film YBCO film, we used an identical film with an overlayer of 90nm Ag. In the latter specimen, at energies below 16keV, the LE–μ^+ do not traverse the Ag layer but stop in front of the superconducting surface, thus allowing the measurement of the field distribution outside the surface of the superconductor. On the other hand, by varying the energy, different penetration depths inside the uncapped sample can be chosen. As an example, Figure 35 shows the field distribution at a mean penetration depth of 38nm with an applied field of 5.3mT.

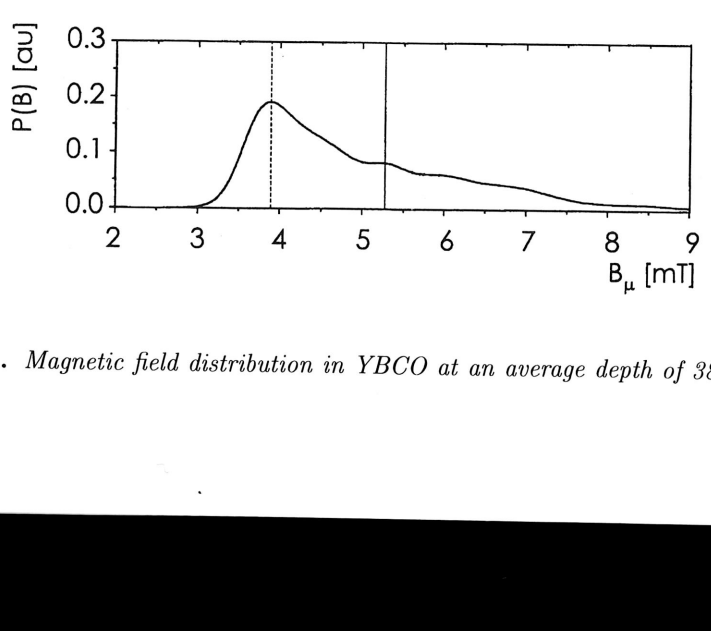

Figure 35. *Magnetic field distribution in YBCO at an average depth of 38nm. B_{ext} = 5.3mT.*

Figure 36 plots the measured values $B_{\text{ext}} - B_{\text{saddle}}$ (at T = 60K, B_{ext}= 5.3mT) versus the mean implantation depth, which has been calculated with the Monte Carlo program discussed in Section 5. The experimental points are compared to the dependence predicted by the depth resolved London model, calculated for different values of the magnetic penetration depth. The data are well described by λ(60 K) ≅180nm , again in good agreement with the results of the depth-independent analysis and show that the London model is able to describe the transition region around the surface of the superconductor in the vortex state.

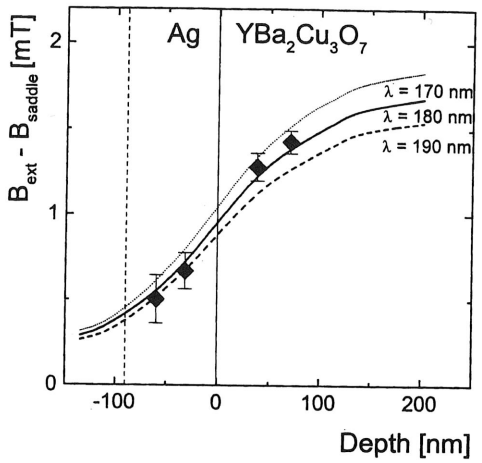

Figure 36. *Plot of as a function of the distance above and below the surface of a YBCO film. The curves are the prediction of the London model for different values of l.*

In conclusion, these experiments provide the first evidence that LE–μ^+ can be used to study microscopic properties such as the distribution of flux inside and near the surface of thin film superconductors. It must be stressed that the data presented have been obtained with reduced statistics (typically about $5\times\ 10^5$). This has to be compared with the 10^7 events generally collected for line shape measurements in the bulk by conventional μSR. Nevertheless, these first results indicate the potential of the LE–μ^+ beam and of depth resolved LE–μSR in the field of HTC superconductors and open the way to future studies.

It is difficult at this stage to give an exhaustive or even just indicative list of possible experiments but a few examples selected among the experiments, which are in preparation or are being actively discussed, may be illustrative. One possible field of future application of LE–μSR is the study of multilayered superconductors. Multilayers have demonstrated to be a very powerful tool for studying the basic physics in semiconductors and metals. Multilayers of superconducting oxides can also be used to probe specific properties of high-Tc superconductors. Particularly interesting is the availability of isostructural insulating ($PrBa_2Cu_3O_7$), conducting ($(Y_{1-x}Pr_x)Ba_2Cu_3O_7$) and superconducting ($REBa_2Cu_3O_7$, RE=Y, Dy, Eu, Er) materials. This large choice of compounds, which have essentially the same lattice parameters and nearly identical growth parameters but very different electronic properties, makes the '123' compounds (materials with the YBCO structure) ideal superlattices constituents (Triscone and Fischer 1997). Questions of interest are the

roles of the individual layer thickness, as well as the coupling between superconducting layers. Another class of experiments, which are made feasible by the availability of a tunable LE–μ^+ beam is the direct determination of magnetic parameters in superconductors such as for instance the penetration depth (Forgan *et al.* 1998). For this, a field is applied parallel to the surface of a thin film. By varying the energy, the μ^+ come to stop at different depths where they detect the local field. From the magnetic field profile the London penetration depth can be obtained. To our knowledge, no other method, at the moment, allows such a direct local measurement of the decay of a field penetrating underneath the surface.

6.4 Magnetic properties of mass selected nanoclusters

Ultra-small metallic particles in the size range 1-10nm (nanoparticles) mark the boundary between molecular and solid state systems and have properties distinct from both. Among the nanoparticles, transition metal particles have considerable potential in various technological fields including high-density magnetic recording, magnetic sensing, catalysis, soft magnetic materials, and ferrofluids. They are currently studied by a number of experimental methods (Dorman and Fiorani 1992). Besides the technological applications, these studies are motivated by the interesting magnetic properties of the particles where a large fraction of atoms are surface atoms. Magnetic nanoclusters behave like a single domain particle with huge magnetic moment $\mu_{np} = N\mu$ (N number of atoms, typically between a few tens to hundreds or thousands, μ atomic moment). Except that a very large moment is involved and that the single atoms of the same cluster are coupled ferromagnetically, the magnetization behavior in thermodynamic equilibrium is identical with that of atomic paramagnetism and the nanocluster assembly behaves as if it was made of giant paramagnetic atoms where the thermal energy plays a significant role in the orientation of the magnetization of each particle. Following this comparison, this phenomenon is called superparamagnetism. For larger particles, the relaxation time associated with thermal agitation is very large, so that the magnetic moments of the particles do not change appreciably during the time scale of the experiment. Small single domain nanoclusters are an almost ideal system with which the phenomenon of superparamagnetism can be studied.

The most commonly used techniques to study superparamagnetism are Mössbauer spectroscopy and ac or dc susceptibility measurements. The μSR technique offers an intermediate observational time window (10^{-5}–10^{-9}s) poorly covered by other methods. Moreover, μSR is not restricted to the investigation of systems containing a sufficient quantity of a Mössbauer element. The unique response to very small magnetic fields makes μSR more sensitive than Mössbauer spectroscopy even for the investigation of dilute Fe nanoclusters. Another difference is that muons sense the field between the nanoparticles (or between the atoms inside the particles), whereas with Mössbauer spectroscopy it is the magnetic field at the nuclei of atoms inside or at the surface of the particles, which is measured. Despite its peculiarities, only very recently the μSR technique has been applied to characterize field distributions and cluster dynamics in superparamagnetic systems (Bewley and Cywinski 1998).

There are various methods for producing nanoparticles. One is evaporation directly onto a substrate with a lower surface free energy such as graphite, which encourages

island growth. Another common way of preparing cluster films is to sputter or evaporate elements simultaneously onto a substrate and then anneal to promote nucleation and segregation. Also precipitation from the solid or from liquid solutions is used. These methods have the advantage of simplicity but produce more or less wide size distributions (generally of lognormal type) with particle separations that vary considerably. Dispersion of sizes and variety of shapes limit the interpretation of the results since many properties depend critically on these parameters.

The use of a gas aggregation source combined with a mass filter allows to produce sufficiently dense assemblies of nanoparticles of transition elements of a well-defined and controllable size in clean UHV conditions (Baker *et al.* 1997). A further advantage with respect to the nanoparticles produced by other methods and investigated up to now, is that the aggregation source produces very pure clusters of unique chemical and homogenous structural composition, thus avoiding the interpretation difficulties introduced by the presence of impurities (that can amount to 10%) or of other structural or magnetic components. Moreover, no oxidation or formation of foreign surface layers takes place during the production. Low energy muons allow μSR studies of well characterized samples of mass selected nanoclusters that can be produced only in the form of thin films. This subject is an example for investigations, where LE–μ^+ are necessary because of the reduced thickness of the system to be studied, but variable implantation depth is not required.

We investigated a 500nm thick mosaic sample of Fe-nanoclusters embedded in a very pure Ag matrix (volume concentration 0.1%) produced in a gas aggregation source (Binns 1997). With a kinetic energy of 16keV, μ^+ penetrate about 70nm into the sample. The implanted μ^+ sense the Fe cluster moments indirectly via the distribution of dipolar magnetic fields resulting from the cluster ensemble. To reduce the sample preparation time, for this preliminary experiment, the clusters were deposited without mass selection (diameter 2.4±0.4nm). Measurements in a transverse magnetic field of 25mT were taken at various temperatures and the muon spin relaxation fitted by a stretched exponential

$$G_x(t) = C \exp\left[-(\lambda t)^{\beta}\right]. \tag{30}$$

The obtained relaxation rate is plotted as a function of the inverse temperature in Figure 37. At low temperatures a constant, large, exponential relaxation ($\beta = 1$) is observed. This behavior reflects a static distribution of dipoles producing a Lorentzian field distribution for the spatial components of the internal field. Such a distribution is also expected according to the treatment of dilute magnetic dipoles of Walstedt and Walker (1974)

$$\lambda_{\mathrm{st}} = \gamma_\mu \Delta B. \tag{31}$$

where ΔB is the half width at half maximum of the Lorentz distribution and is equal to 0.53±0.05mT in the present case. Above 15° K, the relaxation rate decreases with increasing temperature and the relaxation function develops into a root exponential ($\beta = 1/2$) distribution. In this temperature range the arrangement of spins is no longer static on the μ^+ time scale and the relaxation reflects the collective fluctuation of the atomic dipoles. Uemura *et al.* (1985) have shown that for a system of dilute spins in which the spatially averaged field has a Lorentzian distribution, the functional form of the muon depolarisation in an external transverse magnetic field is root exponential in the limit of fast fluctuating atomic moments, *i.e.*

$$G_x(t) = \exp\left[-(\lambda t)^{0.5}\right], \tag{32}$$

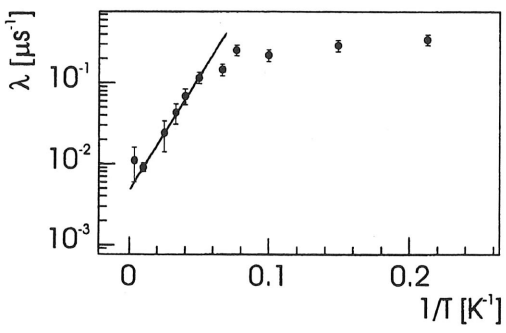

Figure 37. *Muon spin relaxation rate as a function of temperature of 16keV μ^+ implanted in a sample of Fe nanoclusters. An external transverse field of 25mT is applied.*

where $\lambda = 4\gamma_\mu^2 \Delta B^2 \tau$ and τ^{-1} is the fluctuation frequency of the spins.

Figure 37 shows that for temperatures above 15°K (which defines the so-called blocking temperature, *i.e.* the temperature where the spin dynamics as seen by the μ^+ is blocked) the temperature dependence of the relaxation follows closely an Arrhenius law and that the direction of the magnetic moments of the nanoclusters fluctuates spontaneously with a relaxation time given by

$$\tau = \tau_0 \exp\left[E_a/kT\right], \tag{33}$$

where E_a is an activation energy and τ_0 is the inverse of the attempt frequency. By fitting the data above the blocking temperature with an expression of the form given by Equation 33, LE–μSR measurements allow the determination of E_a and . One obtains $\tau_0 = 1.2 \pm 0.2 \times 10^{-8}$s , a value much larger than generally assumed, and $E_a/k_B = 63.5 \pm 3.5$°K. The activation energy is the energy barrier which must be overcome when the magnetization direction flips from one minimum to another. It is determined by contributions from the magnetic anisotropy energy, which determines the preferential orientation of the magnetization and from the energy in the external magnetic field. Therefore, from the measurement of E_a it is possible to quantify the magnetic anisotropy constant.

Anisotropic contributions come from the external shape of the particle, stresses imposed by the matrix, or the crystalline structure itself. By using a simple model of a uniaxial total asymmetry, an effective magnetic anisotropy constant for the investigated Fe-nanoclusters $K_{\text{eff}} \cong 2 \times 10^5 \text{J/m}^3$ is estimated. This is much larger than the value of the cubic anisotropy constant K_1 ($\approx 0.5 \times 105$ J/m^3)for α–Fe, which is expected if magnetocrystalline anisotropy would be dominant. The increase over the bulk value indicates the influence of surface effects on the magnetic properties and a possible deviation of the nanoclusters from the spherical shape.

Equation 33 has been originally proposed by Néel (1949) to describe fluctuations by thermal activation over a single-energy barrier. The result from the LE–μSR measurement is interesting since the problem of the thermal fluctuations of the magnetic moments of a singLE–domain ferromagnetic particle and its decay toward thermal equilibrium, despite much theoretical work after the original theory of Néel and Brown (1963), still presents

several unsolved problems. For instance, the limits of validity of the model are unclear and the dependence of the exponential prefactor on several parameters, *e.g.* , temperature, external field, magnetic moment, and anisotropy constant has never been studied. Recently, experimental studies of magnetization reversal in individual nanosized Ni, Co and Dy particles at low temperatures (Wernsdorfer *et al.* 1997) as well as theoretical investigations of the relaxation time of the magnetic moments of single domain particles without and with external field have reactivated the interest in this field (Coffey *et al.* 1998). Our experiments show that it is possible to study the temperature dependence of nanocluster dynamics in the superparamagnetic state by LE–μSR and that this technique can be used to extract parameters such as activation energy, anisotropy energy and relaxation times of an identical assembly of particles.

The systematic investigation of mass selected nanoclusters by LE–μSR, complementing the studies of individual cluster fluctuations by SQUID techniques, allows to study the behavior of an ensemble of identical nanoclusters as a function of parameters such as cluster size and shape, concentration, and magnetic properties and address some of the open questions.

7 Conclusions

The objective of this work has been to provide an overview of the work related to the development and use of polarized LE μ^+ beams. We highlighted the study of the characteristics of epithermal muons, obtained by moderation of surface muons, and the physical processes responsible for their generation, which are basilar to the whole development. It appears that only simplest atomic or molecular solids such as the cryocrystals interact so weakly with epithermal muons that these are efficiently moderated and can escape from the solid. The investigations, developments, and experiments presented in this work open the way to the use of slow and very slow muons and to LE–μSR, a new generation of μSR experiments and a field which has been identified as a key area of research in the scientific cases for future muon facilities (Schenck *et al.* 1997). Many challenges remain. For instance, more work needs to be done before the muon can be established as a versatile surface probe. However, the results from the reported first LE–μSR studies on thin film samples represent an important milestone and are sufficient to show that the present technique has considerable potential and can be used to investigate relevant questions of actuality. Higher muon fluxes, which may be obtained at new proposed facilities in Europe, Japan and USA will allow full realization of the potential. Also at existing facilities one can contemplate higher fluxes by schemes involving specially designed muon production targets, dedicated secondary beams and multiple moderator setups. For instance, predeceleration of surface muons and extraction at a few tens of keV from a cyclotron trap (Simons *et al.* 1992) and subsequent moderation could lead to a drastic increase of intensity of epithermal muons. Since the overall efficiency is essentially determined by the ratio $L/\Delta R$ (escape depth of eV muons over stop width of the implanted muons) and $\Delta R \propto p^{3.5}$, a reduction of the muon momentum prior to their implantation would increase the moderation efficiency and the absolute number of epithermal muons. This scheme and possible depolarisation effects during the premoderation process remain to be studied in detail, but an improvement by orders of magnitude in eV yields with respect to the surface μ^+ seems attainable.

Conventional μSR has taken more than 20 years to reach the present state of sophistication and diversity and existing muon techniques will be at least as important in the next 20 years as they are now. We can suppose that novel techniques such as LE–μ^+ and LE–μSR, developed to respond to the new needs of the condensed matter community, will mature and assume a secure place together with the different microscopic probes of matter.

Acknowledgment

Several people have contributed in significant way to the developments and experimental work presented here, as evidenced by the co-authors of the papers cited. I would like to express my sincere thanks to all of them. Particularly, I would like to mention the present group of people at PSI (M. Birke, H. Glückler, A. Hofer, Th. Prokscha, and H.-P. Weber) and the collaboration projects with the University of Birmingham (E. M. Forgan, T. Jackson, T. Riseman), Technical University of Braunschweig (J. Litterst) and the University of Konstanz (Ch. Niedermayer, G. Schatz).

References

Abrikosov A, 1957, *Sov Phys JETP* **5**, 1174.

Aegerter C M and Lee S L, 1997, *Appl Magn Reson* **13**, 75.

Badertscher A, Egan P O, Gladisch M, Greene M, Hughes V W, Mariam F G, Lu D C, zuPutlitz G, Ritter M W, Sanders G, Souder P A, Webeck R, 1985, *Nucl Instr Methods,* **A238**, 200.

Baker S H, Thornton S C, Keen A M, Preston T I, Norris C, Edmonds K W and Binns C, 1997, *Rev Sci Instrum.* **68**, 1853.

Becker K, Kippling G, Schoenherr W D, Schulze W and Toelle V, 1972, Proc. *IVth Int Cryogenic Eng Conference*, Eindoven, 319.

Beer G A, Marshall G M, Mason G R, Olin A, Gelbart Z, Kendall K R, Bowen T, Halverston G P, Pifer A E, Fry C A, Warren J B and Kunselman A R, 1986, *Phys Rev Lett* **57**, 671.

Berberich P, Utz B, Prusseit W and Kinder H, 1994, *Physica* **C219**, 497.

Berger M J *et al.* , 1993, ICRU Report 49, *Stopping Powers and Ranges for protons and Alpha Particles.*

Bewley R I and Cywinski R, 1998, *Phys Rev B.* **58** 11544

Biersack J P and St Mädele, 1982, *Radiation Effects,* **64**, 51.

Binns C, 1997, sample prepared by C. Binns, University of Leicester.

Bohr N, 1948, *Mat Fys Medd Dan Vid Selsk,* **18**, No 8.

Brandt E H, 1988, *Low J Temp Phys.* **73**, 355.

Brewer J, 1998, this volume.

Brown W E, 1963, *Phys Rev* **130**, 1677.

Cherry W, 1958, Ph. D. Thesis Princeton University.

Chu S, Mills A P, Yodh A G, Nagamine K, Miyake Y, Kuga T, 1988, Phys. *Rev Lett* **60**, 101.

Coffey W T, Crothers D R S, Dormann J L, Kalmykov Yu P, Kennedy E C, and Wernsdorfer W, 1998, *Phys Rev Lett* **80**, 5655.

Dorman J L and Fiorani D, 1992, Editors, *Magnetic Properties of Fine particles*, North-Holland, Amsterdam.

Eckstein W, 1991, *Computer Simulation of Ion-Solid Interactions*, Springer-Verlag Berlin.

Eder K, Semrad D, Bauer P, Golser R, Maier P-Komor, Aumayr F, Mñalba Pe, Arnau A, Ugalde J M and Echenique P M, 1997, *Phys Rev Lett* **79**, 4112.
Fleming D G, Mikula R J and Garner D M, 1982, *Phys Rev* **A26**, 2527.
Forgan E M, Jackson T, Hückler Gl, Morenzoni E, Prokscha Th *et al.* , 1998, Birmingham-PSI proposal.
Fuchs A, 1992, Ph. D. Thesis ETH-Zürich.
Fuchs A, Prusseit W, Berberich P, Kinder H, 1996, *Phys Rev* **B53**, 14745.
Golser R and Semrad D, 1991, *Phys Rev Lett* **66**, 1831.
Gonin M, Kallenbach R and Bochler P , 1994, *Rev Sci Instrum* **65**, 648.
Gullikson E M, Henke B L, 1989, *Phys Rev* **B39**, 1.
Harshman D R, Warren J B, Beveridge J L, Kendall K R, Kiefl R F, Oram C J, Mills A P, Crane W S, Rupaal A S, Turner J H, 1986, *Phys Rev Lett* **56**, 2850.
Harshman D R, Mills A P, Beveridge J L, Kendall K R, Morris G D, Senba M, Warren J B, Rupaal A S and Turner J H, 1987, *Phys Rev* **B36**, 8850.
Herlach D, Majer G, Rosenkranz J, Schmolz M, Schwarz W, Seeger A, Templ W, Brandt E H, Essmann U, Fürderer K and Gladish M, 1990, *Hyp. Int.* **63** *41.*
Hofer A, 1998, Ph.D. Thesis, Universität Konstanz.
Jääskeläinen J, Laine T, Köm F, Saarinen K and Pärvi H, 1997, *Appl Surf Sci,* **116**, 73.
Kawata J and Ohya K, 1994, *Nucl Instr Methods* **B90**, 29.
Keller H, 1990, in *Earlier and recent aspects of superconductivity*, Bednorz J G, Küller M, Springer Verlag.
Kinder H, 1997, samples prepared by H Kinder, Technical University München.
Krasnoperov E, Meilikhov E, Abela R, Herlach D, Morenzoni E, Gygax F N, Schenck A and Eschenko D, 1992, *Phys Rev Lett* **69**, 1560.
Lee S L, Zimmermann P, Keller H, Warden M, Savic I, Schauwecker R, Zech D, Cubitt R, Forgan E M, Kes P H, Li T W, Menkowski A A and Tarnawski Z, 1993, *Phys Rev Lett* **71**, 3862.
Lee S L, 1998, this volume.
Long M W and Forgan E M, 1997, unpublished.
Matsushita A and Nagamine K, 1996, *Chem Phys Lett,* **253**, 407.
Mayer M and Eckstein W, 1994, *Nucl Instrum and Meth* **B94**, 22.
Mills Jr A P and Crane W S , 1984, *Phys Rev Lett* **53**, 2165.
Mills Jr A P, Imazato J, Saitoh S, Uedono A, Kawashima Y and Nagamine K, 1986, *Phys Rev Lett* **56**, 1463.
Mills Jr A P and Gullikson E M, 1986, *Appl Physics Letters* **49**, 1121.
Mills Jr A P Voris S S and Andrew T S, 1994, *Appl J Phys,* **76**, 2556.
Miyake Y, Shimomura K, Mills A P and Nagamine K, 1997, *Hyp Int* **106**, 237.
Morris G D, 1990, Master of Science Thesis, University of British Columbia.
Morenzoni E, Kottmann F, Maden D, Matthias B, Meyberg M, Prokscha Th, Wutzke Thand Zimmermann U, 1994, *Phys Rev Lett* **72**, 2793.
Morenzoni E, Birke M, Hückler Gl, Hofer A, Litterst J, Meyberg M, Niedermayer C, Prokscha Th, Schatz G and Wutzke Th, 1997, *Hyp Int* **106**, 229.
Morenzoni E, Prokscha Th, Hofer A, Matthias B, Meyberg M, Wutzke Th, Birke M, Hückler Gl, Litterst J, Niedermayer C and Schatz G, 1997, *Appl J Phys,* **81**, 3340.
Nagamine K, 1987, *At Phys* **10**, 225.
Nagamine K, Miyake Y, Shimomura K, Birrer P, Marangos J P, Iwasaki M, Strasser P and Kuga T, 1995, Phys Rev Lett **74**, 4811.
Nakai Y, Shirai T, Tabata T and Ito R, 1987, *At Data Nucl Data Tables,* **37**, 69.
M L Néel, 1949, *Ann de Géophysique,* **5**, 99.
Petkov M P, Lynn K G, Roellig L O and Troev T D, 1997, *Appl Surf Sci,* **116**, 13.
Phelps A V, 1992, *Phys J Chem Ref Data,* **21**, 883.

Pifer A E, Bowen T and Kendall K R, 1976, *Nucl Instr and Methods* **135**, 39.
Prokscha Th, Morenzoni E, Meyberg M, Wutzke Th, Matthias B, Fachat A, Jungmann K and zuPutlitz G, 1998, *Phys Rev* **A58**, 3739.
Rainford B D and Daniel G J, 1994, *Hyperfine Int* **87**, 1129.
Riseman T M, Brewer J H, Chow K H, Hardy W N, Kiefl R F, Kreitzman S R, Liang R, MacFarlane W A, Mendels P, Morris G D, Rammer J, Schneider J W, Niedermayer C and Lee S L, 1995, *Phys Rev* **52**, 10569.
Rudd M E, Toburen L H and Stolterfoth N, 1979, *At Data Nucl Data Tables* **23**, 405.
Rudd M E, Kim K Y, Madison D H and Gallagher J W, 1985, *Rev Mod Phys* **57**, 965.
Schenck A, Cywinski R and Roduner E, *Case study for a muon facility at the European Spallation Source.*
Schou J, 1987, *Nucl Instr and Meth* **27**, 188.
Schultz P J, Lynn K J, 1988, *Rev Mod Physics,* **68**, 701 and references therein.
Schulze W and Kolb D M, 1974, *Faraday Trans II: Chemical Physics,* **70**, 1098.
Senba M, 1988, *Phys J B: Mol Opt Phys* **21**, 3093.
Simons L, Morenzoni E and Kottmann F, 1992, in *Exotic Atoms in Condensed Matter*, Benedek G, Schneuwly H eds., *Springer Proceedings in Physics* **59**, 33.
Storchak V, Brewer J H and Eschenko D, 1997, *Appl Magn Reson* **13**, 15.
Storchak V, this volume (1998.)
Taqqu D, 1986, *Nucl Instr Methods,* **A247**, 288
Thomas E W, Janev R K and Smith J, 1992, *Nucl Instrum and Meth* **B69**, 427.
Käger T, Bucci C, deRenzi R, Jungmann K *et al.* , 1998, private communication.
Triscone M J and Fischer O, 1997, *Rep Prog Phys* **60**, 1673.
Uemura Y, Yamazaki T, Harshman D R, Senba M and Ansaldo E J, 1985, *Phys Rev* **B31**, 546.
Uemura Y J, 1991, *Physica C* **185–189**, 733.
Uemura Y J, 1998, this volume.
Utz B, Semerad R, Bauer M, Prusseit W, Berberich P and Kinder H, 1997, IEEE *Transactions on Applied Superconductivity,* **7**, 1272.
van der Meer S, 1985, *Rev Mod Phys* **57**, 689.
Walstedt R E and Walker L P, 1974, *Phys Rev* **B9**, 4857.
Wernsdorfer W, Bonet Orozco E, Hasselbach K, Benoit A, Barbara B, Demoncy N, Loiseau A, Pascard H and Mailly D, 1997, *Phys Rev Lett,* **78**, 1791.
Yang Q, O'Connor D J and Wang Z , 1991, *Nucl Instr And Meth* **B61**, 149.
Ziegler J F, Biersack J P and Littmark U, 1985, The Stopping and Range of Ions in solids, Vol 1, Pergamon Press New York.